Article

Cancer Cell

Inhibition of TRF1 Telomere Protein Impairs Tumor Initiation and Progression in Glioblastoma Mouse Models and Patient-Derived Xenografts

Graphical Abstract

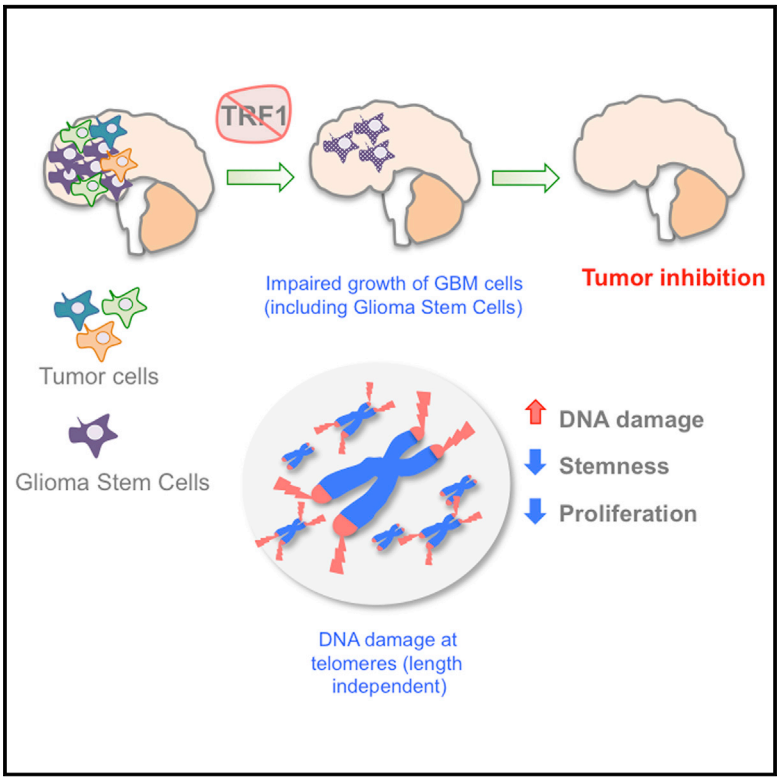

Authors

Leire Bejarano,
Alberto J. Schuhmacher,
Marinela Méndez, ..., Joaquín Pastor,
Massimo Squatrito, Maria A. Blasco

Correspondence

mblasco@cnio.es

In Brief

Bejarano et al. show that genetic or chemical inhibition of TRF1 increases telomeric DNA damage and reduces proliferation and stemness independent of telomere length. TRF1 inhibition also inhibits glioblastoma initiation and progression and prolongs survival in genetic and xenograft glioblastoma models.

Highlights

- TRF1 expression is increased in both human and mouse GBM
- TRF1 inhibition impairs GBM initiation and progression in different mouse models
- The mechanism involves telomeric DNA damage induction and reduced stemness
- TRF1 chemical inhibitors inhibit xenograft growth from patient-derived primary GSCs

Bejarano et al., 2017, Cancer Cell *32*, 590–607
November 13, 2017
https://doi.org/10.1016/j.ccell.2017.10.006

CellPress

CellPress

Cancer Cell
Article

Inhibition of TRF1 Telomere Protein Impairs Tumor Initiation and Progression in Glioblastoma Mouse Models and Patient-Derived Xenografts

Leire Bejarano,[1] Alberto J. Schuhmacher,[2] Marinela Méndez,[1] Diego Megías,[3] Carmen Blanco-Aparicio,[4] Sonia Martínez,[4] Joaquín Pastor,[4] Massimo Squatrito,[2] and Maria A. Blasco[1,5,*]

[1]Telomeres and Telomerase Group, Molecular Oncology Program, Spanish National Cancer Research Centre (CNIO), Melchor Fernández Almagro 3, Madrid, 28029, Spain

[2]Seve-Ballesteros Foundation Brain Tumor Group, Cancer Cell Biology Program, Spanish National Cancer Centre (CNIO), Melchor Fernández Almagro 3, Madrid, 28029, Spain

[3]Confocal Microscopy Unit, Biotechnology Program, Spanish National Cancer Research Centre (CNIO), Madrid, 28029 Spain

[4]Experimental Therapeutics Program, Spanish National Cancer Centre (CNIO), Melchor Fernández Almagro 3, Madrid, 28029, Spain

[5]Lead Contact

*Correspondence: mblasco@cnio.es

https://doi.org/10.1016/j.ccell.2017.10.006

SUMMARY

Glioblastoma multiforme (GBM) is a deadly and common brain tumor. Poor prognosis is linked to high proliferation and cell heterogeneity, including glioma stem cells (GSCs). Telomere genes are frequently mutated. The telomere binding protein TRF1 is essential for telomere protection, and for adult and pluripotent stem cells. Here, we find TRF1 upregulation in mouse and human GBM. Brain-specific *Trf1* genetic deletion in GBM mouse models inhibited GBM initiation and progression, increasing survival. *Trf1* deletion increased telomeric DNA damage and reduced proliferation and stemness. TRF1 chemical inhibitors mimicked these effects in human GBM cells and also blocked tumor sphere formation and tumor growth in xenografts from patient-derived primary GSCs. Thus, targeting telomeres throughout TRF1 inhibition is an effective therapeutic strategy for GBM.

INTRODUCTION

Malignant gliomas represent the majority of primary CNS neoplasms. The most frequent and aggressive glioma is glioblastoma multiforme (GBM) (Louis et al., 2007). Despite all the advances in the molecular characterization of glioblastoma, the median survival has not improved in the last 50 years, being only 14–16 months (Wen and Kesari, 2008).

GBM is known for the high proliferative and infiltrative nature (Chen et al., 2012). GBMs are also highly heterogeneous tumors (Soeda et al., 2015). Cells within the tumor present different expression profiles and may have different responses to radio- and chemotherapy (Bhat et al., 2013). In addition, several studies suggest the existence of a small fraction of cells within the bulk of the tumor with stem-like properties, also termed glioma stem-like cells. These cells are able to recapitulate the original tumor after injection into the brain of immunodeficient mice (Singh et al., 2004). They exhibit radio- and chemoresistant properties, which might explain GBM recurrence after treatment (Bao et al., 2006). This complexity highlights the need for new effective treatments.

Telomeres are heterochromatic structures at the end of chromosomes essential for chromosome stability (De Lange, 2005). Mammalian telomeres are formed by tandem repeats of the TTAGGG sequence bound by the so-called shelterin complex, formed by TRF1, TRF2, POT1, TPP1, TIN2, and RAP1

Significance

Glioblastoma is an incurable tumor mainly owing to its high tumor-initiating cell potential. Telomere maintenance is among the most frequent alterations in human glioblastoma, but if telomeres are good targets to cease GBM growth remains unclear. This study demonstrates that disrupting telomeric capping through direct inhibition of the shelterin protein TRF1 is a promising strategy for treating GBM. We demonstrate that inhibition of TRF1 effectively blocks GBM in both murine and human GBM models. We further demonstrate the striking effectiveness of TRF1 inhibition in impairing the growth of glioma stem cells. These results have a potential impact in cancer treatment as current therapies are unable to kill glioma stem cells and patients die owing to the recurrence of the tumors.

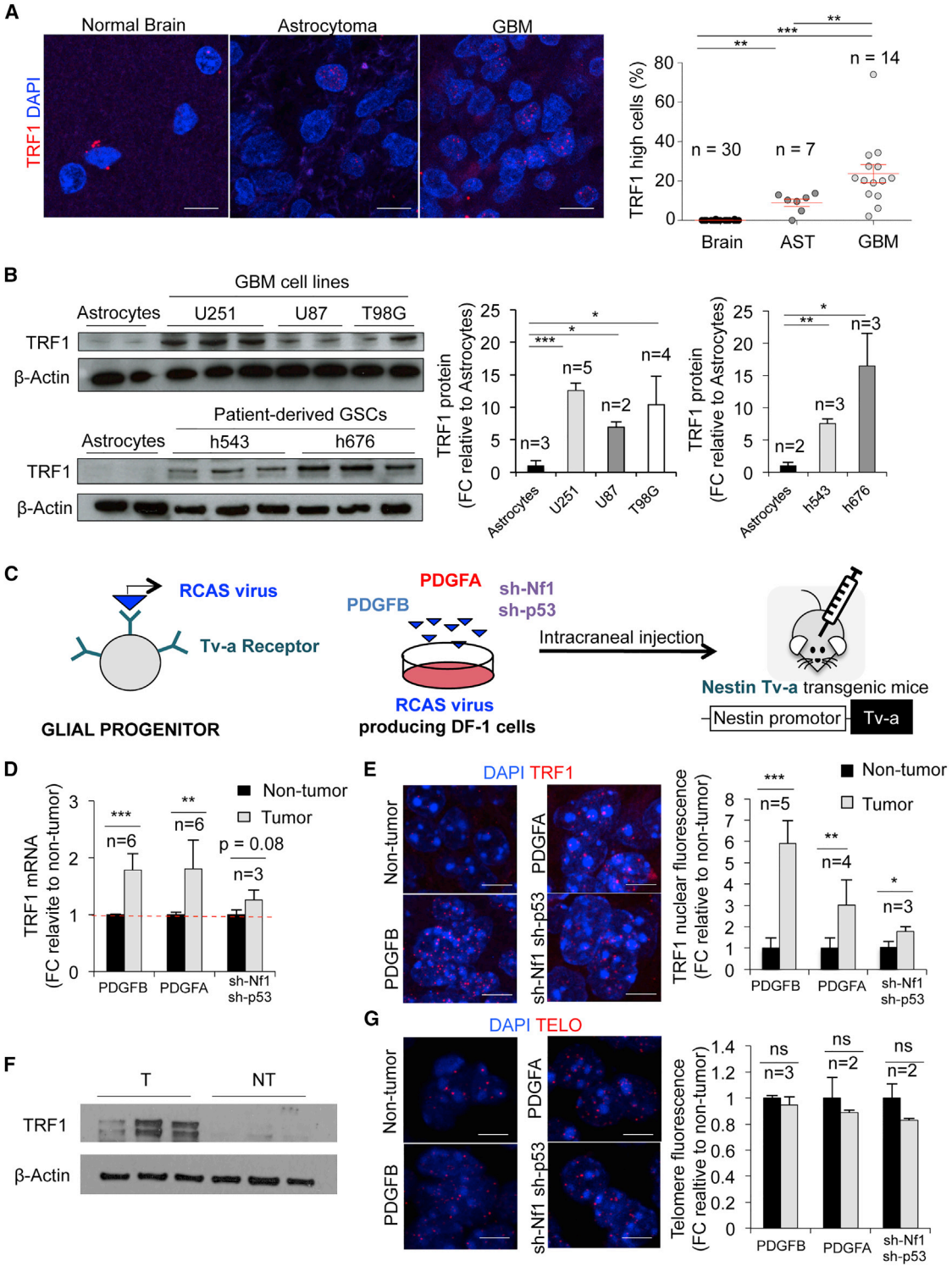

Figure 1. *Trf1* Is Upregulated in Mouse and Human GBM

(A) Representative images (left) and quantification (right) of percentage of cells with high TRF1 expression determined by immunofluorescence. Scale bars, 10 μm.

(B) Western blot images (left) and quantification (right) of TRF1 protein levels in the indicated cells.

(C) Generation of mouse models of GBM by overexpression of PDGFB or PDGFA or by knock down of Nf1 and p53 in Nestin-expressing cells (i.e., glial progenitors).

(D) TRF1 mRNA levels by qRT-PCR in GBM subtypes compared with non-tumor areas.

(E) Quantification of nuclear TRF1 fluorescence in tumor and non-tumor areas and representative images. Scale bars, 5 μm.

(legend continued on next page)

(Liu et al., 2004). With each cell division, telomeres shorten due to the incomplete replication of chromosome ends, a phenomenon known as the "end-replication" problem (Harley et al., 1990). This telomere shortening can be compensated through the *de novo* addition of telomeric repeats by telomerase, a reverse transcriptase composed of a catalytic subunit (TERT) and an RNA component (Terc), used as template for the synthesis of TTAGGG repeats (Greider and Blackburn, 1985). In normal adult cells, however, telomerase is not usually expressed, and telomeres progressively shorten associated to organismal aging (Martínez and Blasco, 2011; Harley et al., 1990).

Telomere maintenance above a minimum length is essential to sustain the indefinite proliferation potential of cancer cells, thus telomeres are considered as potential anti-cancer targets (Hanahan and Weinberg, 2011; Kim et al., 1994). More than 90% of human tumors aberrantly express telomerase (Kim et al., 1994; Shay and Bacchetti, 1997), while the remaining telomerase-negative tumors activate an alternative mechanism to elongate telomeres based on recombination between telomeric sequences, known as ALT (Bryan et al., 1997). The promoter of the *TERT* gene is mutated in 58%–84% of human primary GBMs (Nonoguchi et al., 2013; Boldrini et al., 2006), while pediatric GBMs frequently display an ALT phenotype associated with *ATRX* mutations (Heaphy et al., 2011). These facts highlight the importance of telomere maintenance in glioblastoma and pinpoint telomeres as promising targets. In this regard, most studies have focused on telomerase inhibition. However, telomerase-deficient mice are only cancer resistant when telomeres reach a critically short length (Gonzalez-Suarez et al., 2000) and this effect is lost in the absence of the *Trp53* tumor suppressor gene, which is commonly mutated in cancer (Chin et al., 1999). Clinical trials with telomerase inhibitors have only shown therapeutic benefits in a few myeloid malignancies but have largely failed in solid tumors (El Fassi et al., 2015; Middleton et al., 2014; Parkhurst et al., 2004), maybe as a consequence of telomere length heterogeneity within tumors, which may hamper the effective killing of all tumor cells including the tumor-initiating populations with stem cell-like properties.

Several studies suggest that inhibiting TRF1 could represent an alternative to telomerase inhibitors to target telomeres independently of telomere length. TRF1 directly binds TTAGGG telomere repeats where it is essential for telomere protection (De Lange, 2005; Martínez and Blasco, 2011). *Trf1* deletion *in vivo* induces a persistent DNA damage response (DDR) at telomeres, which is sufficient to block cell division and induce senescence and/or apoptosis in different mouse tissues (Martínez et al., 2009; Beier et al., 2012; Schneider et al., 2013). Interestingly, TRF1 is overexpressed in adult stem cell compartments and in pluripotent stem cells, where it is essential to maintain tissue homeostasis and pluripotency, respectively (Schneider et al., 2013; Boué et al., 2010). TRF1 is also overexpressed in several cancer types such as renal cell carcinoma (Pal et al., 2015) and gastrointestinal tumors (Hu et al., 2010). Furthermore, dominant negative mutations in the TRF1-interacting protein POT1 have been found in different tumor types including familiar glioblastoma cases, again highlighting the importance of telomeres in GBM (Bainbridge et al., 2015; Ramsay et al., 2013; Calvete et al., 2015; Robles-Espinoza et al., 2014). Finally, we recently reported that induction of telomere uncapping by *Trf1* genetic depletion or chemical inhibition can effectively block the growth of aggressive and rapidly growing lung tumors in *Trp53*-deficient *Kras*G12V mice, in a manner that is independent of telomere length (García-Beccaria et al., 2015), thus further supporting that TRF1 could be a good anti-cancer target for aggressive tumors.

Here, we set to address whether TRF1 inhibition blocks GBM growth in both *in vivo* mouse models and human xenograft models, and to address whether these effects occur independently of telomere length.

RESULTS

TRF1 Is Overexpressed in Both Human and Mouse GBM

We first addressed whether TRF1 expression is altered in human and mouse GBM. For this, we analyzed TRF1 protein levels by immunofluorescence in a total of 30 normal human brains, 7 astrocytomas, and 14 GBMs. The percentage of cells presenting high TRF1 levels was highest in GBMs, followed by astrocytomas, while TRF1 was almost undetectable in normal brain tissue (Figure 1A). We validated these results by determining TRF1 total protein levels by western blot in three independent human GBM cell lines and in two patient-derived primary glioblastoma stem cell (GSC) cultures. Again, TRF1 protein expression was significantly increased in all three human GBM cell lines (U251, U87, and T98G) and in the two patient-derived primary GSCs cultures (h543 and h676) compared with primary astrocytes (Figure 1B). TRF2 and RAP1 protein levels were also found upregulated in the patient-derived primary GSCs compared with normal astrocytes (Figure S1A). This upregulation of different shelterin proteins in human GBM cells compared with normal astrocytes, seemed to occur at the post-transcriptional level as we did not find significant differences in the mRNA levels of different shelterins when using qRT-PCR (Figure S1B).

Next, we studied TRF1 expression in various mouse models of GBM generated by specifically targeting Nestin-expressing cells with RCAS vectors carrying different oncogenic insults in Nestin-Tva transgenic mice. Neural stem cells (NSCs) express Nestin, and, thus, these cells are targeted by the different oncogenic insults. In particular, we generated mice with different GBM subtypes by either overexpressing PDGFB or PDGFA in a *Cdkn2a* null background, or by knocking down Nf1 and p53 in a wild-type background (Figures 1C and S1C–S1F). PDGFA overexpression results in proneural-like GBMs, while PDGFB and sh-Nf1 sh-p53 induced glioblastomas with a mesenchymal signature (Ozawa et al., 2014) (Figures S1C–S1F). TRF1 mRNA levels were significantly upregulated in the three mouse GBM

(F) Western blot for TRF1 protein levels in PDGFB tumors (T) and non-tumor (NT) areas.

(G) Telomere Q-FISH analysis of tumor and non-tumor areas. Scale bars, 5 μm.

Data are represented as the mean ± SD with the exception of 1A, which is the mean ± SEM. n represents the number of independent human samples in (A), the number of biological replicates in (B), and the number of mice in (D–G). Statistical analysis: unpaired t test. *p < 0.05, **p < 0.01, ***p < 0.001. See also Figures S1 and S2.

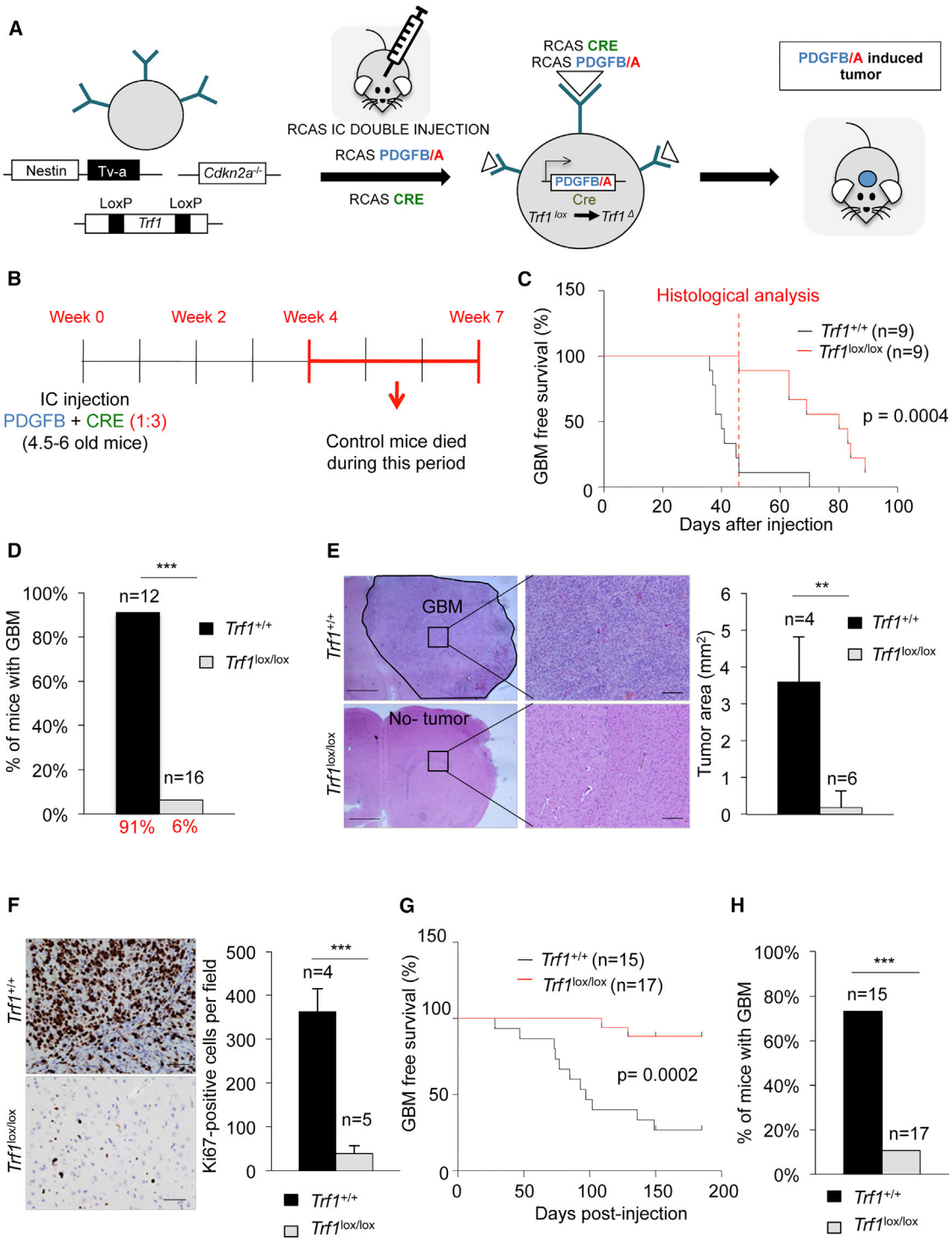

Figure 2. *Trf1* Deletion Impairs Tumor Initiation in Various GBM Subtypes

(A) GBM are induced by PDGFB overexpression simultaneously with Cre expression to delete the $Trf1^{lox}$ allele, specifically in Nestin-expressing cells.

(B) Schematic representation of the experimental procedures.

(C) Survival curves of mice with the indicated genotypes. Histological analysis is performed 45 days after tumor induction in a different cohort of mice.

(D) Percentage of mice with GBM 45 days after tumor induction.

(E) Representative images (left) and quantification (right) of tumor area by H&E at 45 days after tumor induction. Scale bars, 500 μm (left) and 200 μm (right).

(F) Representative images (left) and quantification (right) of Ki67-positive cells per field at 45 days after tumor induction. Scale bar, 100 μm.

(legend continued on next page)

subtypes, with highest levels in PDGFA- and PDGFB-induced GBM (Figure 1D). The TRF1 protein was also upregulated in all GBM subtypes, again with PDGFB- and PDGFA-induced tumors showing the highest TRF1 levels (Figure 1E). TRF1 protein upregulation was validated by western blot in PDGFB-induced tumors compared with normal tissue (Figure 1F).

Next, we addressed whether other shelterin components, namely TRF2, RAP1, POT1, TPP1, and TIN2 (Liu et al., 2004), were also upregulated in mouse GBM models. TPP1, POT1, and TIN2 mRNA levels were slightly higher in the three GBM subtypes by qRT-PCR, but the differences did not reach statistical significance with the exception of TIN2 upregulation in PDGFB-induced GBM and TPP1 upregulation in PDGFA-induced tumors (Figure S1G). RAP1 was significantly downregulated in PDGFB and PDGFA-induced tumors and TRF2 did not change in any of the GBM subtypes (Figure S1G).

To assess whether higher TRF1 levels were the consequence of longer telomeres in tumors compared with normal tissue, we measured telomere length by quantitative telomere FISH (Q-FISH) in the different mouse GBM subtypes. We did not find any significant differences in telomere length between tumors and non-tumoral tissue in any of the GBM subtypes (Figure 1G). This is in agreement with previous findings showing that high TRF1 levels in pluripotent and adult stem cells are uncoupled from telomere length (Marion et al., 2009; Tejera et al., 2010; Schneider et al., 2013). We next studied whether TRF1 levels correlated with the well-known stem cell markers SOX2, NESTIN, CD133, and MYC, using the Gliovis data portal for analysis of GBM expression datasets (Bowman et al., 2017). We found a positive correlation between TRF1 levels and all the stem cell markers with the exception of MYC (Figures S2A–S2D), although TRF1 was positively correlated with the MYC modulator USP13 (Fang et al., 2017) (Figure S2E). These findings suggest that TRF1 overexpression in GBM is not the simple consequence of longer telomeres in these tumors, but instead may reflect their high cancer stem cell nature as TRF1 is upregulated in stem cells and pluripotent stem cells (Lathia et al., 2015; Schneider et al., 2013). In summary, all three mouse GBM subtypes upregulate TRF1 in a manner that is independent of telomere length.

Trf1 Genetic Deletion Impairs Tumor Initiation in Different Mouse GBM Subtypes

We next set to genetically validate TRF1 as a potential anti-cancer target in the GBM subtypes studied here. We first studied the impact of *Trf1* abrogation in the PDGFB-induced GBM model, as it showed the highest TRF1 overexpression. To this end, we crossed Nestin-Tva;*Cdkn2a*$^{-/-}$ mice with *Trf1* inducible knockout mice (Martínez et al., 2009) to obtain *Trf1*$^{lox/lox}$;Nestin-Tva;*Cdkn2a*$^{-/-}$ or *Trf1*$^{+/+}$;Nestin-Tva;*Cdkn2a*$^{-/-}$ mice (Figure 2A). Then, we injected, intracranially into the subventricular zone (SVZ) of adult mice (4.5–6 weeks), the RCAS-PDGFB DF-1-producing cells together with RCAS-Cre-producing cells to simultaneously delete *Trf1* in a 1:3 ratio (the number of RCAS-Cre-producing cells was three times higher than the RCAS-PDGFB-producing cells). This results in overexpression of PDGFB in glial progenitors simultaneously with Cre-mediated *Trf1* excision specifically in these cells (Figures 2A, 2B, and S1D), allowing assessment of the impact of *Trf1* abrogation on tumor initiation. We validated *Trf1* excision by injecting RCAS-Cre-producing DF-1 cells into the brain of 2 days old pups, as the percentage of Nestin-expressing cells is higher in newborns (Mignone et al., 2004). PCR, qRT-PCR, and immunofluorescence analysis of the brain 2 days after injection confirmed TRF1 downregulation in *Trf1*$^{lox/lox}$ mice compared with controls (Figures S3A–S3C). In the setting of *Cdkn2a* deficiency, tumors started to appear 4–5 weeks after intracranial injection (Ozawa et al., 2014) (Figure 2B).

Strikingly, even in this setting of fast-growing tumors, mice with *Trf1*-deleted brains showed an increased survival of 80% compared with the *Trf1*$^{+/+}$ controls (Figure 2C). At time of death, *Trf1*-deleted tumors were histological indistinguishable from *Trf1*$^{+/+}$ tumors and showed normal TRF1 mRNA and protein levels, indicating that they were escapers (Figures S3D–S3F). Telomere Q-FISH analysis also revealed that all the tumors had the same telomere length (Figure S3G). The fact that no tumors lacking TRF1 expression were found suggests that TRF1 is essential for PDGFB-induced GBM initiation.

To study the cellular and molecular effects of *Trf1* deletion in GBM initiation, we killed the mice at an earlier time point before they started dying from GBM (i.e., 45 days after tumor induction). At this time point, 91% of *Trf1*$^{+/+}$ mice showed brain tumors compared with only 6% of *Trf1*$^{lox/lox}$ mice (Figure 2D). Histological analysis revealed a significant difference in tumor size between both genotypes, with *Trf1*$^{lox/lox}$ tumors being undetectable by H&E staining in most of the cases (Figure 2E). Immunohistochemistry analysis of the human astrocyte (HA) tag, which marks PDGFB-expressing cells in this model, also confirmed smaller *Trf1*$^{lox/lox}$ tumors compared with controls (Figure S3H). Finally, *Trf1*$^{lox/lox}$ brains showed very few proliferating cells compared with a high proliferation index in *Trf1*$^{+/+}$ tumors (Figure 2F), indicating impaired tumor growth by *Trf1* deletion.

Similar results were obtained in the PDGFA-induced mouse model of GBM, where tumors grow more slowly than in the PDGFB model. In this case, *Trf1*$^{lox/lox}$ mice showed a highly significant 65% increase in survival compared with *Trf1*$^{+/+}$ mice (Figures 2A and 2G). In particular, by day 150 after tumor induction around 75% of *Trf1*$^{+/+}$ mice had already died from GBM, while only 10% of *Trf1*$^{lox/lox}$ mice were affected (Figure 2H).

Trf1 Deficiency Leads to Telomeric Damage and Reduced Stemness in Primary NSCs

To study how *Trf1* deletion impairs GBM initiation, we addressed the cellular and molecular effects of abrogating *Trf1* specifically on isolated NSCs. NSCs express Nestin, and, thus, these cells are the targets of the RCAS vectors when we perform the intracranial injections into the SVZ of Nestin-Tva mice. To this end, we established an *in vitro* system using

(G) Survival curve of mice of the indicated genotypes injected with PDGFA-producing DF-1 cells.
(H) Percentage of mice affected with GBM 150 days after tumor induction; same cohort as (G).
Data are represented as mean ± SD. n represents the number of mice. Statistical analysis: unpaired t test, log rank test, and chi-square test. **p < 0.01, ***p < 0.001. See also Figure S3.

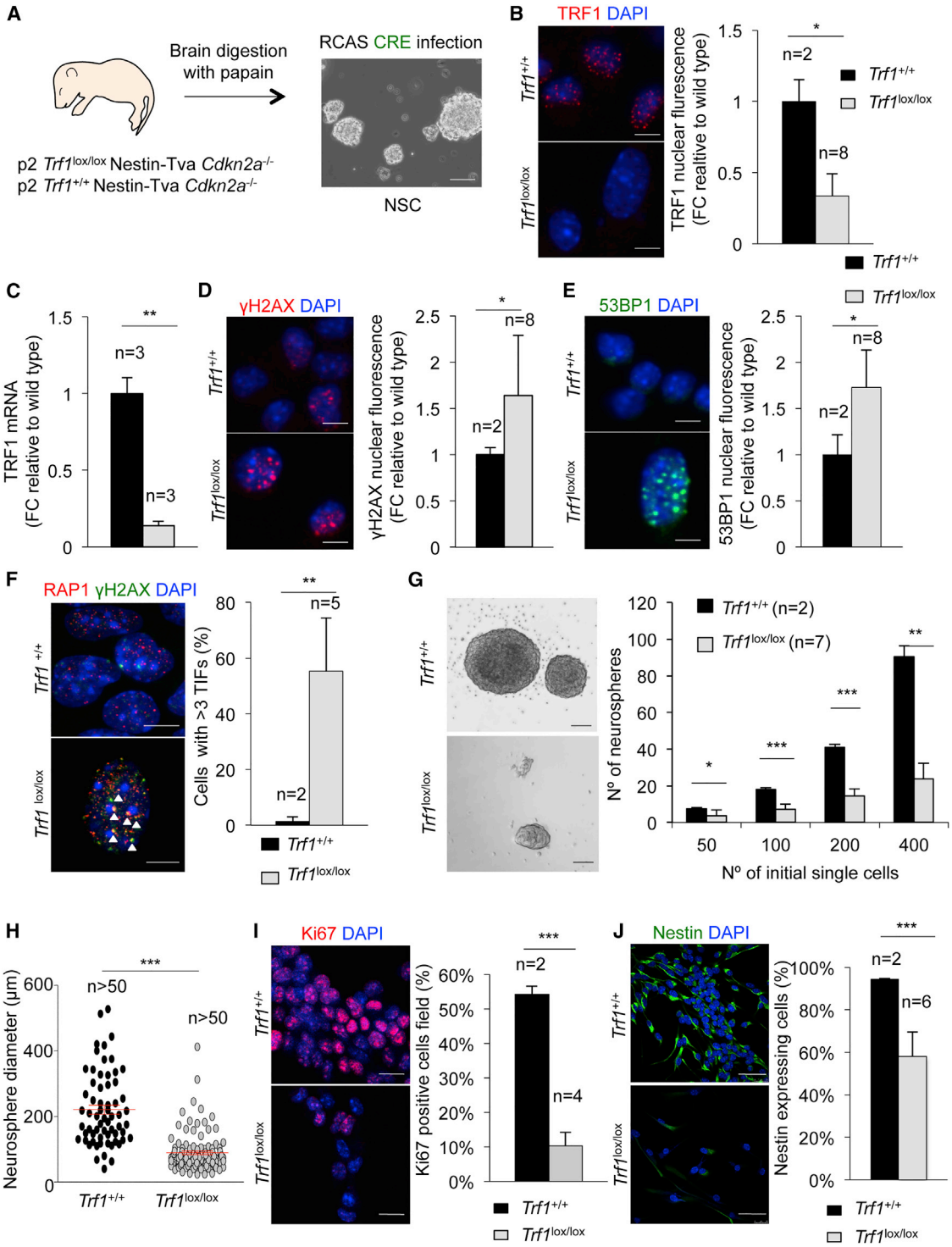

Figure 3. *Trf1* Abrogation Induces DNA Damage and Reduced Stemness in NSCs

(A) NSCs are obtained by digestion of brain of 2-day-old pups from the indicated genotypes with papain. *Trf1* allele is depicted by Cre-mediated excision. Scale bar, 100 μm.

(B) Representative images (left) and quantification (right) of TRF1 protein levels determined by TRF1 immunofluorescence in $Trf1^{+/+}$ and $Trf1^{lox/lox}$ NSC. Scale bars, 5 μm.

(C) TRF1 mRNA levels by qRT-PCR in $Trf1^{+/+}$ and $Trf1^{lox/lox}$ NSC.

(D) Representative images (left) and quantification (right) of γH2AX nuclear intensity in $Trf1^{+/+}$ and $Trf1^{lox/lox}$ NSCs 5 days after the last RCAS-Cre infection. Scale bars, 5 μm.

(legend continued on next page)

primary NSCs isolated from *Trf1*$^{+/+}$ *and* *Trf1*$^{lox/lox}$ Nestin-Tva *Cdkn2a*$^{-/-}$ newborn brains (2 days old) (Figure 3A). To induce *Trf1* deletion, we transduced two independent lines of *Trf1*$^{+/+}$ and eight independent lines of *Trf1*$^{lox/lox}$ primary NSC with the RCAS-Cre virus. We confirmed downregulation of both TRF1 mRNA and protein by qRT-PCR and by immunofluorescence, respectively, in *Trf1*$^{lox/lox}$ primary NSC compared with the *Trf1*$^{+/+}$ controls (Figures 3B and 3C).

Trf1 deletion has been previously shown to induce a persistent DDR at telomeres in both fibroblasts and epithelial cells (Martínez et al., 2009). To address whether *Trf1* deletion also leads to DNA damage in NSCs, we quantified 53BP1 and γH2AX levels by immunofluorescence in *Trf1*-deficient NSC compared with *Trf1*$^{+/+}$ controls. We found significantly higher γH2AX and 53BP1 nuclear fluorescence intensities in *Trf1*$^{lox/lox}$ NSC compared with *Trf1*$^{+/+}$ controls (Figures 3D and 3E). In addition, double immunofluorescence staining of γH2AX and the telomeric protein RAP1 showed increased DNA damage specifically located at telomeres (the so-called telomere induced foci or TIFs) in the case of *Trf1*-deleted NSC compared with *Trf1*$^{+/+}$ controls (Figure 3F), indicating that telomeres were being uncapped as the consequence of *Trf1* deletion, leading to a DDR at telomeres.

As TRF1 expression is upregulated and it is essential for both adult stem cells and pluripotent stem cells (Schneider et al., 2013), we next studied the impact of *Trf1* deletion on the stem potential of NSC. To this end, we performed a neurosphere formation assay by disaggregating NSCs from *Trf1*$^{+/+}$ and *Trf1*$^{lox/lox}$ brains and plating single cells in serial dilutions. Both the number and diameter of secondary neurospheres were significantly decreased in *Trf1*-deficient NSC compared with *Trf1*$^{+/+}$ controls (Figures 3G and 3H). This was accompanied by a significant reduction of the Ki67 proliferation marker (Figure 3I) and a reduction of percentage of Nestin-positive cells (Figure 3J). In summary, *Trf1* deletion in NSC induces a DDR at telomeres and reduces stemness in NSCs, probably reducing the tumor-initiating potential of these cells upon oncogenic transformation.

Therapeutic Effects of *Trf1* Abrogation in Already Established GBMs

To validate TRF1 as a therapeutic target that could be translated into human patients, we next generated additional mouse models in which we could first induce the different GBM subtypes and then delete *Trf1* once the tumors were established. To this end, we crossed *Trf1*$^{lox/lox}$;Nestin-Tva;*Cdkn2a*$^{-/-}$ or *Trf1*$^{+/+}$;Nestin-Tva;*Cdkn2a*$^{-/-}$ mice with *hUBC-CreERT2* mice to obtain *Trf1*$^{lox/lox}$;Nestin-Tva;*Cdkn2a*$^{-/-}$;*hUBC-CreERT2* and *Trf1*$^{+/+}$;Nestin-Tva;*Cdkn2a*$^{-/-}$;*hUBC-CreERT2,* which allowed for ubiquitous Cre-induced *Trf1* deletion upon tamoxifen administration once the tumors had formed. We first induced tumors with PDGFB, and 2.5 weeks after tumor induction we started the treatment with tamoxifen to delete *Trf1* in the whole organism (Figures 4A and 4B). At this time point tumors had already started to form (Figure S4A).

Trf1$^{lox/lox}$-deleted mice showed a 33% increase in survival compared with *Trf1*$^{+/+}$ mice (Figure 4C), suggesting therapeutic effectiveness of *Trf1* deletion in reducing GBM tumor growth once the tumors were already established. Furthermore, we found that 25% of the GBM tumors appearing in *Trf1*-deleted mice were escapers as they showed normal TRF1 expression, and were excluded from further analyses (Figures S4B and S4C), again highlighting the potent anti-tumorigenic effect of *Trf1* deletion.

To better study the effects of *Trf1* abrogation in already established tumors, we killed the mice at an earlier time point (32 days after tumor induction). We found a 50% decrease in TRF1 protein fluorescence in *Trf1*$^{lox/lox}$ tumors compared with *Trf1*$^{+/+}$ controls (Figure 4D). Similarly to the tumor initiation models, *Trf1* deletion did not cause any significant change in telomere length in these tumors (Figure S4D), further confirming that the therapeutic effects of *Trf1* deletion consist in direct telomere uncapping in GBM tumor cells independently of their telomere length. Also, we did not find any changes in the mRNA levels of other shelterin components upon TRF1 deletion as determined by qRT-PCR (Figure S4E). Histopathological analysis showed that *Trf1*-deleted tumors were significantly smaller compared with the controls (Figure 4E). *Trf1*-deleted tumors also showed significantly less Ki67-positive cells (Figure 4F), indicating lower proliferation.

In addition, we found significantly increased numbers of cells with DNA damage (γH2AX-positive cells) in the *Trf1*-deficient tumors compared with the controls (Figure 4G). This damage was located at telomeres, as indicated by a significantly increased percentage of cells with more than one TIF in *Trf1*-deficient tumors compared with the controls (Figure 4H). Increased telomeric damage was also accompanied by a significant increase in downstream cell-cycle inhibitors p21 and p53 and in the apoptosis marker AC3 (Figure 4I). However, we did not see significant changes in phospho-RPA32 (Figure S4F), indicating that DNA damage is probably independent of the ATR/Chk1 pathway. In summary, *Trf1* deletion in already-formed GBM tumors leads to impaired proliferation and increased telomeric DNA damage.

Similar results were obtained when *Trf1* was deleted in already established tumors that were induced using PDGFA as an independent oncogenic insult. In this case, mice were fed with

(E) Representative images (left) and quantification (right) of 53BP1 nuclear intensity in *Trf1*$^{+/+}$ and *Trf1*$^{lox/lox}$ NSC 5 days after the last RCAS-Cre infection. Scale bars, 5 μm.

(F) Representative images (left) and quantification (right) of percentage of cells presenting three or more γH2AX and RAP1 colocalizing foci (TIFs) 5 days after the last RCAS-Cre infection. White arrowheads: colocalization of γH2AX and RAP1. Scale bars, 5 μm.

(G) Representative images (left) and of number (right) of neurospheres from *Trf1*$^{+/+}$ and *Trf1*$^{lox/lox}$ NSC 1 week after plating. Scale bars, 100 μm.

(H) Quantification of neurosphere diameter from *Trf1*$^{+/+}$ and *Trf1*$^{lox/lox}$ NSC 1 week after plating.

(I) Representative images (left) and percentage (right) of Ki67-positive cells in *Trf1*$^{+/+}$ and *Trf1*$^{lox/lox}$ NSCs. Scale bars, 20 μm.

(J) Representative images (left) and percentage (right) of Nestin-expressing cells. Scale bars, 50 μm.

Data are represented as mean ± SD, with the exception of (H), which is mean ± SEM. n represents independent NSC lines, with the exception of (H), which is the number of neurospheres. Statistical analysis: unpaired t test. *$p < 0.05$, **$p < 0.01$, ***$p < 0.001$.

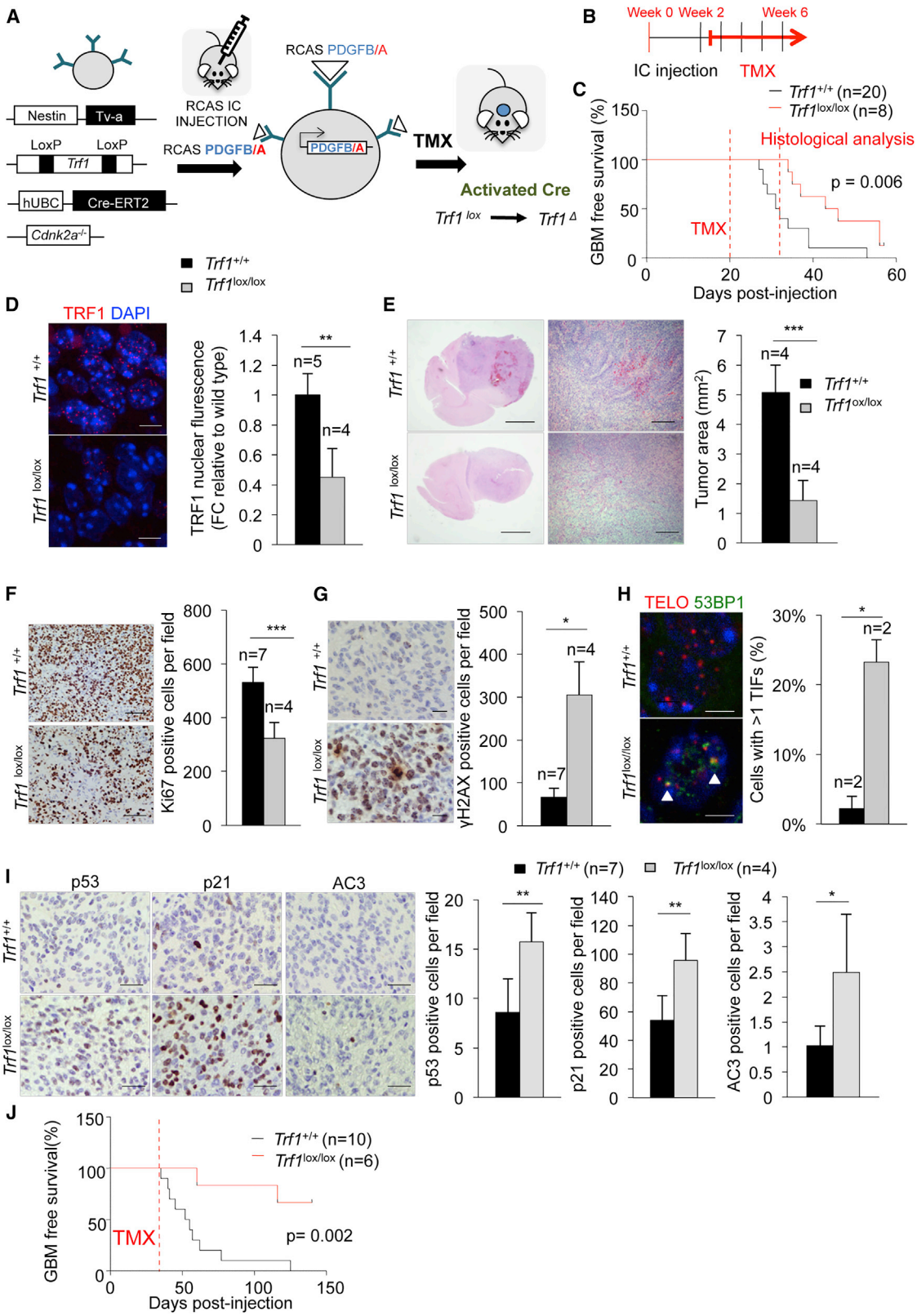

(legend on next page)

tamoxifen 5–6 weeks after tumor induction, whenever the first mice started to die from tumors. Again, *Trf1* deletion post-tumor induction in *Trf1*$^{lox/lox}$ mice resulted in a significant increase in survival compared with *Trf1*$^{+/+}$ mice (Figures 4A and 4J). As in the PDGFB model, *Trf1* deletion was determined by PCR and TRF1 expression was determined by immunofluorescence in all tumors to eliminate all the tumors that did not delete *Trf1* for further analyses (Figures S4G and S4H). In summary, *Trf1* deletion effectively blocks tumor progression in two independent (PDGFB and PDGFA) GBM mouse models concomitant with induction of telomere DNA damage.

Trf1-Deficient GSCs Show Decreased Stemness and Tumorigenicity

To study the effects of *Trf1* abrogation specifically in isolated GSCs from already-formed GBM tumors, we established an *in vitro* system by isolating GSC from *Trf1*$^{lox/lox}$;Nestin-Tva; *Cdkn2a*$^{-/-}$;*hUBC-CreERT2* and *Trf1*$^{+/+}$;Nestin-Tva;*Cdkn2a*$^{-/-}$; *hUBC-CreERT2* mice after tumor induction with PDGFB (Figure 5A). After 15 days of *in vitro* treatment with tamoxifen to delete *Trf1*, PCR analysis of the *Trf1* locus showed a population of *Trf1*^{lox} GSC deleted for *Trf1* (Figure 5B). These *Trf1*-deleted cells showed a significant reduction in both number of neurospheres and diameter of the neurospheres compared with the controls (Figures 5C and 5D).

Next, we studied whether *Trf1* abrogation affected the tumorigenic potential of these cells. Previous studies have shown that GSCs have the ability to form secondary tumors after orthotopic injection into the brain of syngeneic mice (Jiang et al., 2011). Thus, we injected *Trf1*$^{+/+}$ and *Trf1*$^{lox/lox}$ GSC into the brain of syngeneic mice fed with tamoxifen to induce *Trf1* deletion (Figure 5E). Mice injected with *Trf1*$^{lox/lox}$ GSC showed a significant increase in survival compared with the controls (Figure 5F), indicating that *Trf1* deletion significantly decreased the ability of GSC to form secondary GBM tumors. Moreover, 120 days after GSC injection, 71% of mice injected with *Trf1*$^{+/+}$ GSC had died owing to secondary tumors compared with only 10% of the mice injected with *Trf1*$^{lox/lox}$ GSC (Figure 5G). Postmortem histological analysis showed that the secondary tumors were histologically similar to the parental PDGFB-induced tumors, from which cells were extracted (Figure 5H); thus, *Trf1* abrogation in GSCs strongly reduces their stemness and tumor forming potential.

Brain-Specific or Whole-Body *Trf1* Deletion in Mice Does Not Significantly Impair Memory, Neuromuscular, and Olfactory Functions

Previous studies showed that *Trf1* whole-body deletion in adult mice was compatible with mouse viability, although highly proliferative compartments such as the skin and the bone marrow showed decreased cellularity (García-Beccaria et al., 2015). Similarly, deletion of *Terf2*, which encodes another essential shelterin component in adulthood, does not lead to brain dysfunction (Lobanova et al., 2017). To validate TRF1 as a safe target in the treatment of GBM, we set to address whether brain-specific or whole-body *Trf1* deletion would affect the brain functions of mice.

We first checked TRF1 expression in the normal brain. In agreement with increased TRF1 expression in adult stem cells in mice (Schneider et al., 2013), we found significant TRF1 expression in the SVZ compared with cerebral cortex (Figure 6A). The SVZ is one of the main areas of adult neurogenesis, characterized by the expression of the stem cell marker Nestin (Faiz et al., 2015). Next, as the percentage of Nestin-positive cells is higher in newborns (Mignone et al., 2004), we injected RCAS-Cre virus-producing DF-1 cells to induce *Trf1* deletion into the brain of *Trf1*$^{lox/lox}$;*Cdkn2a*$^{-/-}$ and *Trf1*$^{+/+}$;*Cdkn2a*$^{-/-}$ newborns (2 days old) (Figure 6B) and let these mice reach adulthood to assess any neurological effects of TRF1 deletion (see Figures S3A–S3C for brain TRF1 levels). When mice reached adulthood, around 2.5 months after RCAS-Cre-producing DF-1 cell injection, PCR analysis confirmed that four out of the six mice still showed *Trf1* deletion in the brain (Figure S5). Thus, decreased TRF1 levels specifically in the brain are maintained to adulthood without resulting in decreased mouse viability.

To address whether *Trf1* depletion in newborn brains affected adult brain function, we performed different tests to measure cognitive and olfactory capacities, memory, coordination, and balance. Olfactory capacities were measured by using the so-called buried food test, in which mice were fasted 24 hr and then moved to a new cage with a buried food pellet (Yang and Crawley, 2009) (Figure 6C). Mice of both genotypes were able to find the food pellet with a 100% success rate (Figure 6D). The time used to find the pellet was also similar in *Trf1*$^{+/+}$ and *Trf1*$^{lox/lox}$ mice (Figure 6E). Next, we evaluated the memory skills by using the object recognition test (Bernardes de Jesus et al., 2012). We first trained the mice by placing them in a box with two identical objects (A and A), and then we changed one of

Figure 4. *Trf1* Deletion Delays Tumor Progression in PDGFB-Driven GBM

(A) Schematic representation of tumors induced by PDGFB overexpression and *Trf1*^{lox} allele deletion generated by tamoxifen treatment after tumors are formed.
(B) PDGFB-producing cells are injected to induce tumors. At 2.5 weeks after tumor induction mice are treated with tamoxifen. Mice start dying from GBM at week 4 after treatment.
(C) Survival curves of the indicated genotypes. Histological analysis is performed 32 days after tumor induction in a different cohort of mice.
(D) Representative images (left) and quantification (right) of TRF1 nuclear fluorescence intensity at 32 days after tumor induction. Scale bars, 5 μm.
(E) Representative images (left) and quantification (right) of tumor areas by H&E at 32 days after tumor induction. Scale bars, 1 mm (left) and 100 μm (right).
(F) Representative images (left) and number (right) of Ki67-positive cells per field in tumors at 32 days after tumor induction. Scale bars, 100 μm.
(G) Representative images (left) and number (right) of γH2AX-positive cells per field in *Trf1*$^{+/+}$ and *Trf1*$^{lox/lox}$ tumors at 32 days after tumor induction. Scale bars, 20 μm.
(H) Representative images (left) and percentage (right) of cells presenting one or more 53BP1 and telomere colocalizing foci (TIFs). White arrowheads: colocalization of 53BP1 and telomeres. Scale bars, 5 μm.
(I) Representative images (left) and percentage (right) of p53-, p21-, and AC3-positive cells. Scale bars, 50 μm.
(J) Survival curves of mice of the indicated genotypes injected with PDGFA-producing cells.
Data are represented as mean ± SD. n represents the number of mice. Statistical analysis: unpaired t test and log rank test. *p < 0.05, **p < 0.01, ***p < 0.001. See also Figure S4.

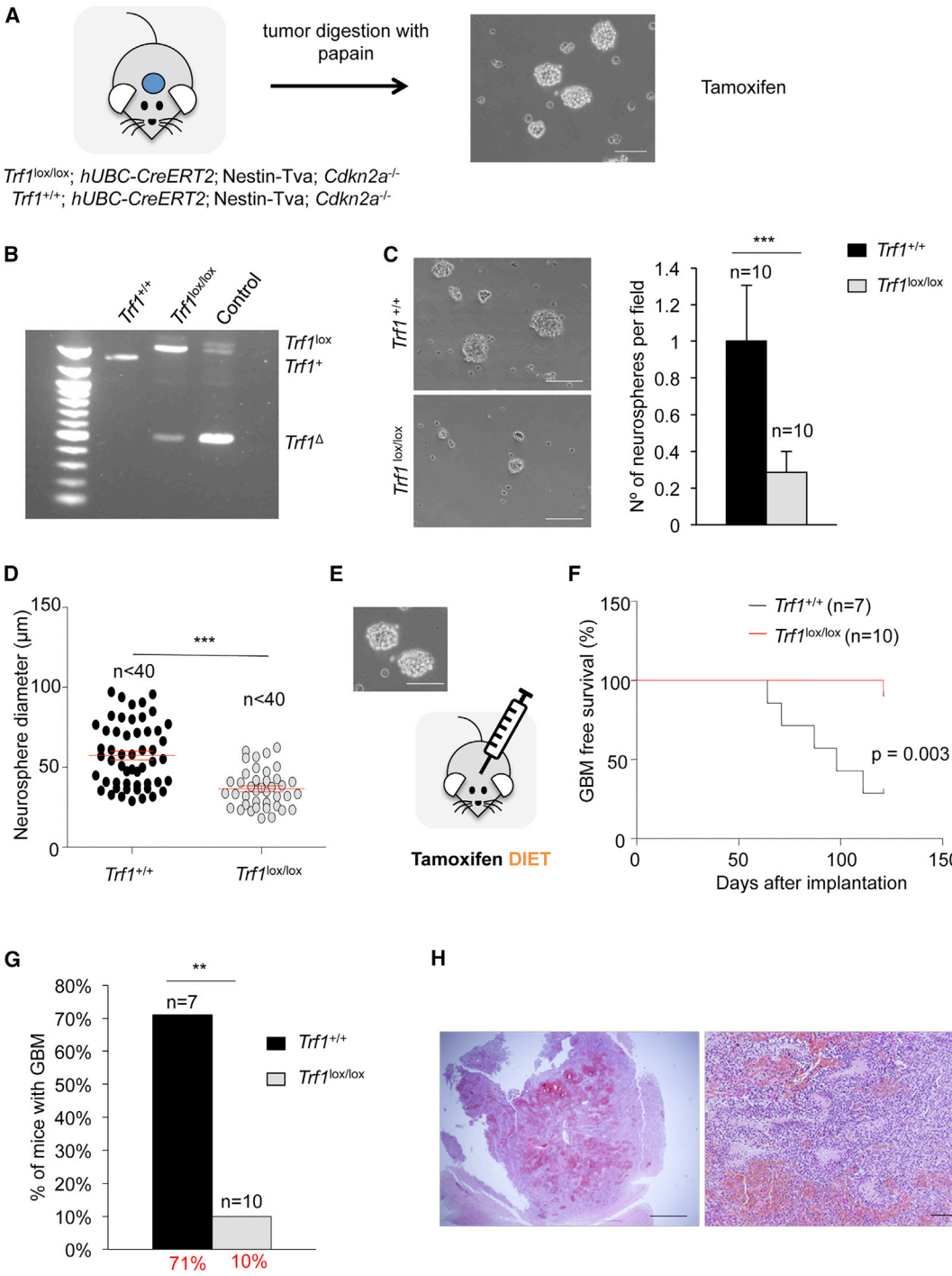

Figure 5. *Trf1*-Deficient Glioma Stem Cells Show Reduced Stemness and Reduced Tumor Forming Potential

(A) $Trf1^{+/+}$ and $Trf1^{lox/lox}$ GSCs are obtained by tumor digested with papain. The $Trf1^{lox}$ allele is generated by tamoxifen treatment. Scale bar, 100 µm.

(B) Analysis of *Trf1* excision by PCR.

(C) Representative images (left) and number (right) of neurospheres from $Trf1^{+/+}$ and $Trf1^{lox/lox}$ GSC. Scale bars, 100 µm.

(D) Quantification of neurosphere diameter from $Trf1^{+/+}$ and $Trf1^{lox/lox}$ GSC.

(E) GSCs are orthotopically injected in syngeneic mice fed with tamoxifen. Scale bar, 100 µm.

(F) Survival curves of mice injected with $Trf1^{+/+}$ and $Trf1^{lox/lox}$ GSCs.

(G) Percentage of mice affected by the injection of $Trf1^{+/+}$ and $Trf1^{lox/lox}$ GSCs.

(H) Representative image of $Trf1^{+/+}$ tumor histology. Scale bars, 500 µm (left) and 100 µm (right).

Data are represented as mean ± SD with the exception of (D), which is the mean ± SEM. n represents the number of fields in (C), the number of spheres in (D), and the number of mice in (F and G). Statistical analysis: unpaired t test and log rank test. **p < 0.01, ***p < 0.001.

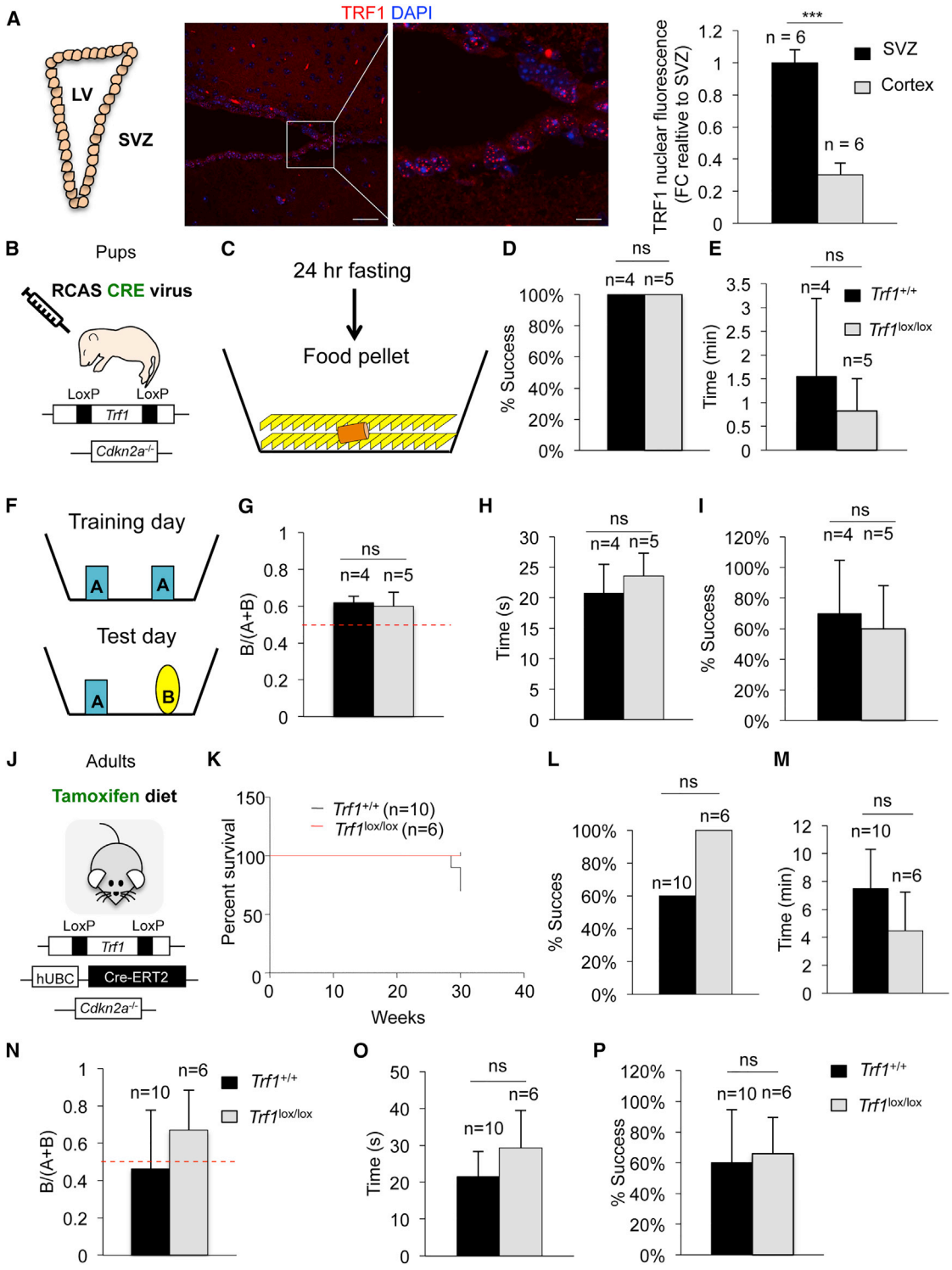

Figure 6. *Trf1* Brain-Specific Deletion in Healthy Mice Does Not Compromise Brain Function of Organism Viability

(A) Representative images (left) and quantification (right) of TRF1 nuclear fluorescence in the SVZ compared with the surrounding cerebral cortex. Scale bars, 50 μm (left) and 10 μm (right).

(B) *Trf1* deletion is induced by Cre-mediated recombination in 2-day-old newborns.

(C) After 24 hr fasting, mice are moved to a cage with a buried food pellet and both the success and the time to find the pellet are measured.

(D and E) Percentage of success finding the pellet (D) and time needed to find the pellet (E).

(F) Mice were trained in a box with two identical objects (A). The test day one of the object was changed (B).

(legend continued on next page)

the objects on the day of the test (A and B) (Figure 6F). By calculating the time spent with the new object B and by dividing this by the time spent with (A + B), which is an indication of the memory skills, we observed no significant differences between genotypes (Figure 6G). To evaluate coordination and balance we performed two independent tests, the rotarod and the tight rope (Bernardes de Jesus et al., 2012; Tomás-Loba et al., 2008). In the rotarod test we measured the time mice could stay on the rod. In the tightrope test, we evaluated the ability of the mice to stay on the rope without falling, and we considered the test a "success" if mice were able to stay on the rope for more than 1 min. No significant differences were found between *Trf1*$^{+/+}$ and *Trf1*$^{lox/lox}$ mice in any of these two tests (Figures 6H and 6I).

In parallel, to address the effects of whole-body *Trf1* deletion in adult mice, we fed 10 week old *Trf1*$^{lox/lox}$;*Cdkn2a*$^{-/-}$;*hUBC-CreERT2* and *Trf1*$^{+/+}$;*Cdkn2a*$^{-/-}$;*hUBC-CreERT2* mice tamoxifen (Figure 6J). These mice with whole-body *Trf1* deletion present a normal survival up to at least 7 months of age (Figure 6K). After 2 months of continuous treatment, we performed the buried food test, the object recognition test, and the rotarod and tightrope tests, and found no significant differences between *Trf1* wild-type and *Trf1*-deleted mice (Figures 6L–6P), demonstrating that *Trf1* deletion in the brain does not affect cognitive, olfactory, memory, or neuromuscular abilities of the mice.

TRF1 Inhibition Reduces Stemness and Proliferation and Increases Telomeric Aberrations and DNA Damage in Human GBM Cells

We previously reported the discovery of small molecules that can inhibit TRF1 telomeric foci (García-Beccaria et al., 2015). To address whether they show therapeutic effects in GBM, we first treated U251 human GBM cells with the TRF1 inhibitors, ETP-47228, ETP-47037, and ETP-50946 (Figure 7A). Immunofluorescence analysis to quantify TRF1 foci intensity revealed that the three compounds effectively reduced TRF1 nuclear foci fluorescence by approximately 50% compared with DMSO-treated cells (Figure 7B). We also confirmed reduced TRF1 protein levels by western blot analysis (Figure 7C). Similar to TRF1 genetic depletion, TRF1 chemical inhibitors significantly reduced proliferation (Figure 7D) and induced DNA damage, as determined by 53BP1 levels (Figure S6A). To assess whether the DNA damage was specifically located at telomeres, we determined the abundance of TIFs. To this end, we performed a double immunofluorescence of γH2AX with the telomeric protein RAP1, which showed that the percentage of cells with two or more TIFs was significantly increased upon treatment with the TRF1 chemical inhibitors (Figure 7E).

Next, we set to address whether TRF1 chemical inhibitors also reduced stemness of human GBM cells. To this end, we cultured U251 cells with NSC medium to obtain a suspension culture enriched in stem cells, and performed a sphere formation assay upon treatment with ETP-47228, ETP-47037, and ETP-50946, or DMSO, for 7 days. Treated cells showed a strong reduction in both number and diameter of neurospheres compared with the controls (Figures 7F and S6B).

To discard possible off-target effects of TRF1 chemical inhibitors, we knocked down TRF1 by small hairpin RNA in the U251 GBM cell line (Figures S6C and S6D). Similar to chemical inhibition, TRF1 knocked down cells showed decreased proliferation (Figure S6E) and increased DNA damage markers γH2AX and 53BP1 (Figure S6F). We also observed an increase in the so-called multitelomeric signals (Figure S6G), a telomere aberration previously associated to loss of TRF1 (Martínez et al., 2009; Sfeir et al., 2009). Also, similar to TRF1 chemical inhibition, the number and diameter of the neurospheres was significantly decreased in TRF1 knocked down cells compared with the controls (Figures S6H and S6I). Thus, TRF1 genetic inhibition mimics the effects shown by TRF1 chemical inhibition in human GBM cells.

TRF1 Chemical Inhibition Synergizes with γ-Irradiation and Temozolomide to Reduce Proliferation of Human GBM Cells

The standard of care for GBM patients consists of surgical resection combined with radiation and chemotherapy, as well as adjuvant chemotherapy. Unfortunately, frequent recurrences after treatment are observed owing to their radio- and chemoresistant properties (Bhat et al., 2013; Bao et al., 2006). Dysfunctional telomeres have been shown to lead to increased radiosensitivity, most likely as the consequence of telomere uncapping (Goytisolo et al., 2000; Alt et al., 2000). In addition, low levels of telomerase expression are shown to correlate with a higher sensitivity to temozolomide (TMZ), indicating that telomeres may play a role in TMZ resistance (Kanzawa et al., 2003). As both genetic and chemical TRF1 inhibition significantly impairs GBM proliferation and stemness concomitant with induction of a DDR at telomeres, we set to study the combined effects of simultaneous TRF1 inhibition and γ-irradiation or TMZ treatments in human U251 GBM cells. Upon irradiation, glioma cells predominantly arrest in the G_2/M phase (Badie et al., 1999) (Figure 7G). Combined TRF1 chemical inhibition and γ-irradiation (6 Gys) synergistically increased the percentage of G_2 arrested cells (Figure 7G). These effects were also recapitulated in TRF1 knocked down cells (Figure S7A). We also observed a synergistic effect of TRF1 inhibitors with irradiation in increasing DNA damage, as determined by γH2AX levels and colocalization of γH2AX with the telomeric protein RAP1 (Figures 7H and S7B). Combined TRF1 inhibition and TMZ treatment for 3 days also synergistically reduced cell viability

(G) Quantification of time spent with B/(A + B).
(H) Time spend in the rotarod.
(I) Percentage success in the tightrope.
(J) *Trf1* whole-body deletion is induced by tamoxifen diet from the age of 10 weeks.
(K) Survival curves of mice of the indicated genotypes.
(L and M) Percentage of success finding the pellet (L) and time needed to find the pellet (M).
(N) Quantification of time spent with B/(A + B).
(O) Time spend in the rotarod.
(P) Percentage success in the tightrope.
Data are represented as mean ± SD. n represents the number of mice. Statistical analysis: unpaired t test. ns, not significant. ***$p < 0.001$. See also Figure S5.

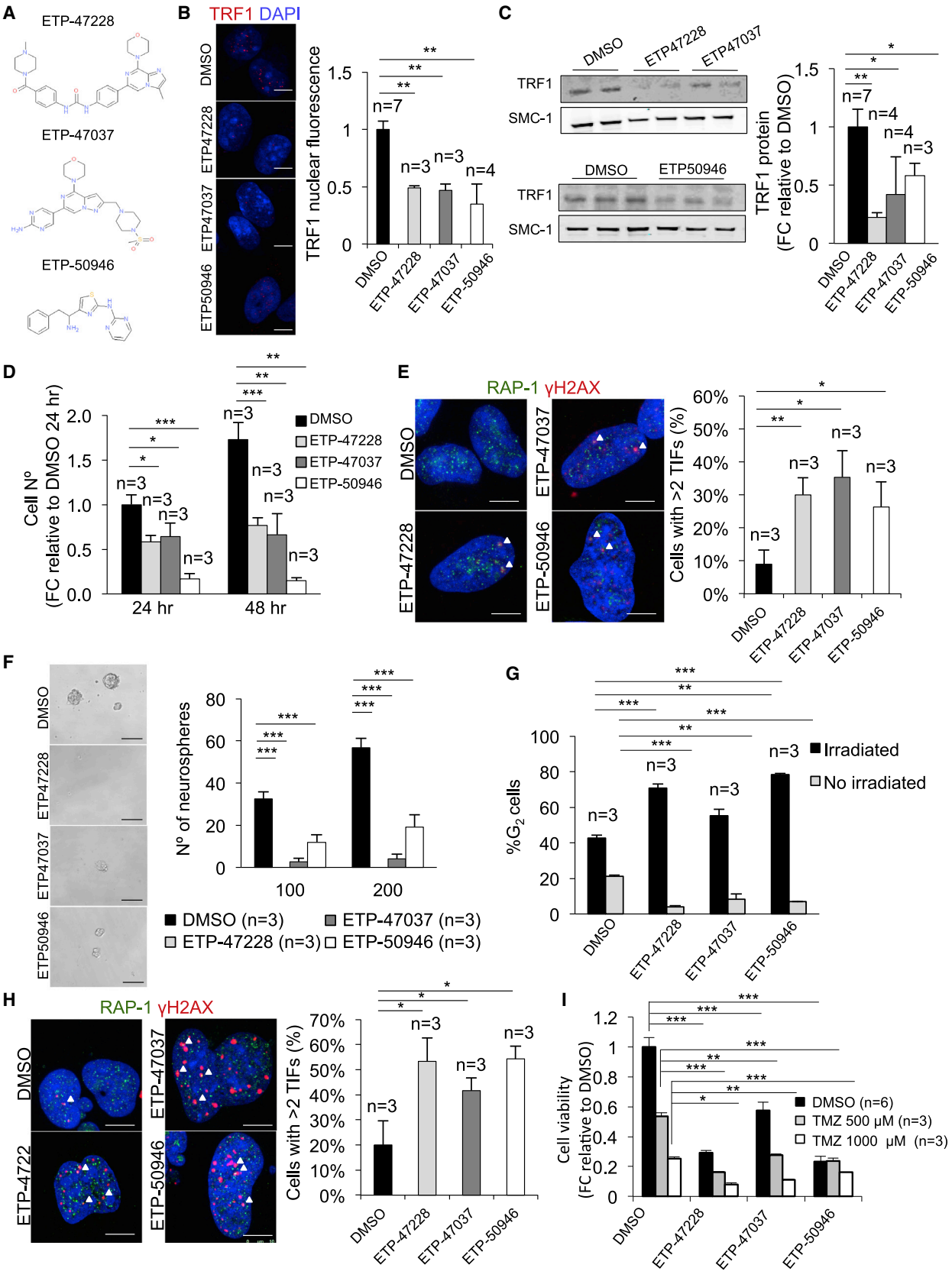

(legend on next page)

in U251 GBM cells (Figure 7I), thus suggesting that TRF1 inhibition synergizes with current standard treatments for GBM.

TRF1 Chemical Inhibition Reduces Stemness and Xenograft Tumor Growth of Patient-Derived Primary GSCs

To validate the TRF1 chemical inhibitors in a more relevant clinical setting, we treated two independent patient-derived primary GSCs (h543 and h676) cultures with the TRF1 inhibitors. Again, treatment of h543 and h676 cells with the three inhibitors revealed a significant reduction in both the number and diameter of spheres compared with the untreated controls (Figures 8A, S8A, and S8B).

As the TRF1 inhibitors cannot cross the blood-brain barrier, we next injected h676 and h543 cells subcutaneously into nude mice and treated them with orally administered TRF1 inhibitors. One week after GSC injection, mice received oral administration of the vehicle as placebo or ETP-47037 5 days/week, every week until human endpoint, and tumors were continuously followed up by caliper measurements (Figure 8B). Xenografts from h676 GSCs and those treated with ETP-47037 showed a drastic reduction in tumor area compared with vehicle-treated mice at all time points after treatment until the placebo group reached the human endpoint (Figure 8C). Xenografts from h543 GSCs showed slower tumor growth, but again ETP-47037-treated mice showed decreased tumor growth compared with the vehicle, which was maintained until vehicle-treated mice were killed owing to very large tumors (Figure 8D).

Postmortem tumor analysis of xenografts from h676 GSCs revealed a striking decrease in tumor size and tumor weight in the ETP-47037-treated tumors compared with those treated with the placebo (Figure 8E). TRF1 immunofluorescence analysis confirmed that tumors treated with ETP-47037 showed an 80% reduction in TRF1 protein levels (Figure 8F). This TRF1 reduction was accompanied by a decrease in the proliferation marker Ki67 (Figure 8G) and an increase in the DNA damage marker γH2AX (Figure 8H). In addition, full histological analysis revealed that, while placebo-treated tumors showed high cellularity, open chromatin, active nucleus, and mitotic cells, ETP-47037-treated tumors were characterized by low cellularity, compacted chromatin, fragmented DNA, apoptotic bodies, and necrotic areas (Figure S8C).

Of relevance, we did not observe any signs of sickness or morbidity in the ETP-47037-treated cohorts compared with the placebo group, in agreement with a therapeutic window for TRF1 inhibition (García-Beccaria et al., 2015). Histological analysis of the mice did not reveal any deleterious effects of ETP-47037 treatment in the highly proliferative tissues, including the skin, intestine, and bone marrow (Figure S8D). Only one mouse out of four showed a mild widening of lymphatic vessels in the intestine (Table S1). In summary, TRF1 chemical inhibitors effectively reduce number and diameter of neurospheres *in vitro* in two independent patient-derived primary GSC cultures. Furthermore, oral administration of TRF1 inhibitors to patient-derived xenograft models using primary GSCs, drastically impairs tumor growth.

DISCUSSION

GBM remains an incurable tumor, with a mean survival of less than 2 years from diagnosis (Wen and Kesari, 2008). Recent efforts to understand the genetic origin of GBM have identified telomere maintenance genes (i.e., telomerase) among the most frequently mutated in GBM (Nonoguchi et al., 2013; Boldrini et al., 2006; Heaphy et al., 2011). Telomere maintenance above a minimum length is thought to be necessary for indefinite cancer cell growth (Hanahan and Weinberg, 2011), thus leading to the proposal that inhibition of telomerase may be an anticancer strategy (Kim et al., 1994). However, both telomerase abrogation in mouse cancer models and human clinical trials with telomerase inhibitors have shown limited benefit, as telomerase inhibition only affects cell viability when telomeres are short, and tumors are heterogeneous in terms of telomere length (Middleton et al., 2014; Parkhurst et al., 2004; Gonzalez-Suarez et al., 2000; Chin et al., 1999). In the particular case of GBM, telomere targeting has also focused on direct (Marian et al., 2010) or indirect telomerase inhibition (Hasegawa et al., 2016).

In this study, we investigated an alternative approach to target telomeres by targeting the telomere protective protein TRF1, with which we expected to induce telomere uncapping in every tumor cell, independently of its telomere length. In addition, the fact that TRF1 is enriched in adult stem cell compartments and pluripotent stem cells, and that it is essential for maintenance of tissue homeostasis and pluripotency (Schneider et al., 2013;

Figure 7. TRF1 Chemical Inhibitors Induce DNA Damage and Reduce Stemness in GBM Human Cells

(A) Structure of the chemical compounds ETP-47228, ETP-47037, and ETP-50946.

(B) Representative images (left) and quantification (right) of TRF1 nuclear fluorescence of U251 cells treated with the indicated compounds. Scale bars, 5 μm.

(C) Western blot images (left) and TRF1 protein levels (right) of U251 cells treated with the indicated compounds.

(D) Cell numbers at 24 and 48 hr of U251 cells treated with the indicated compounds.

(E) Representative images (left) and percentage (right) of cells presenting two or more γH2AX and RAP1 colocalizing foci (TIFs). White arrowheads: colocalization of γH2AX and RAP1. Scale bars, 10 μm.

(F) Representative images (left) and quantification (right) of the number of neurospheres formed by U251 cells treated with the indicated compounds. Scale bars, 100 μm.

(G) Percentage of U251 cells in G_2 phase upon 6 Gy irradiation and treated with the indicated compounds.

(H) Representative images (left) and percentage (right) of cells presenting two or more γH2AX and RAP1 colocalizing foci (TIFs) upon 6 Gy irradiation and treated with the indicated compounds. DMSO represents IRR alone. White arrowheads: colocalization of γH2AX and RAP1. Scale bars, 10 μm.

(I) Cell viability measured by an MTT assay in the U251 human cell line treated with the indicated compounds and no temozolomide, temozolomide 500 μM, or temozolomide 1,000 μM for 3 days.

Data are represented as mean ± SD. n represents the number of biological replicates. Statistical analysis: unpaired t test. *$p < 0.05$, **$p < 0.01$, ***$p < 0.001$. See also Figures S6 and S7.

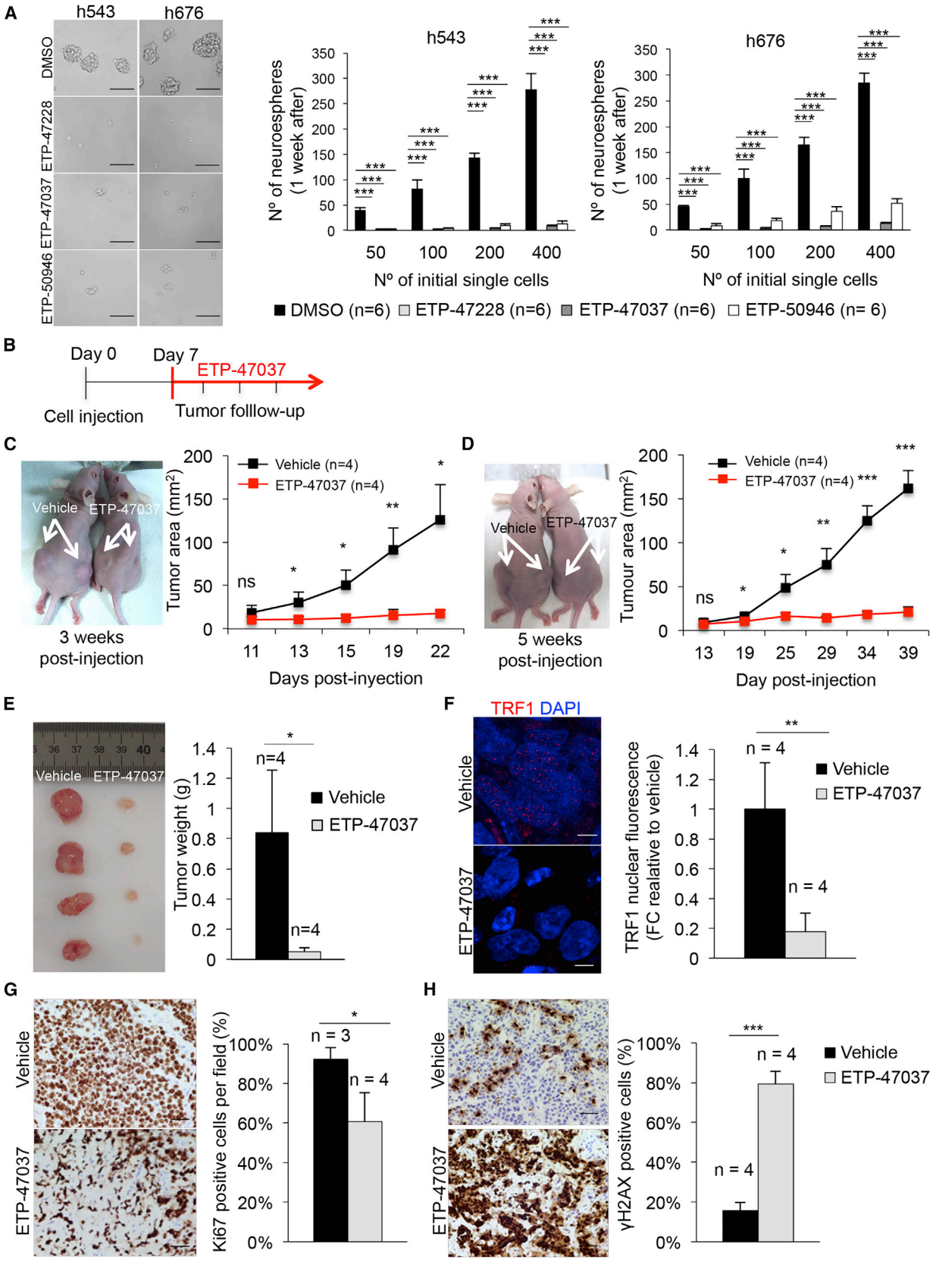

(legend on next page)

Boué et al., 2010), suggests that targeting TRF1 could also impair tumor-initiating capabilities in GBM (Chen et al., 2012).

In line with a role for TRF1 in GBM growth, we found here that TRF1 is overexpressed in both human GBM models (tumor cell lines and patient-derived primary GSCs) and in several GBM mouse models in a manner that is independent of telomere length. We found that TRF1 is also overexpressed in the NSC compartments in the mouse, such as the subventricular zone, which is enriched in Nestin-expressing NSCs, and that TRF1 expression also correlates with the well-known stem cell markers SOX2, CD133, and Nestin in human GBM samples, further reinforcing the notion that TRF1 is upregulated in adult stem cell compartments and required for maintenance of tissue homeostasis (Schneider et al., 2013).

Importantly, we demonstrate here TRF1 is an effective target in GBM by using both genetic ablation mouse models and chemical inhibitors. Genetic deletion of TRF1 effectively blocks both GBM initiation and progression of already established GBM tumors in various mouse models of GBM resulting in a striking increase in survival. As predicted, the therapeutic effect of TRF1 inhibition occurred in a telomere length-independent manner, overcoming the potential problem of telomere length heterogeneity within tumors and the inability to kill all tumor cells, including the tumor-initiating populations. Indeed, *Trf1* deletion reduced the stemness of both NSCs and glioma stem-like cells, at the same time that induced a DDR at telomeres. Of note, in our experimental setting, around 25% of the tumors were escapers and future experiments warrant the study of these potential resistance mechanisms.

TRF1 chemical inhibition recapitulated the findings observed with TRF1 genetic deletion, including decreased TRF1 protein levels, induction of telomere DNA damage located at telomeres, and decreased proliferation and stemness of glioma cells. In particular, TRF1 chemical inhibitors showed a potent blocking effect in sphere formation, thus demonstrating the ability of these inhibitors to block stemness in GBM. Importantly, oral administration of TRF1 chemical inhibitors drastically reduced tumor growth *in vivo* in xenograft mouse models from patient-derived primary GSCs.

We find these observations of potentially clinical relevance, as the recurrence of GBM after the current treatments is due to the resistance of the GSCs and their capability to recapitulate the original tumor. Any potential anti-cancer target, however, must also fulfill the important requisite of not showing deleterious effects in healthy tissues or compromising organism viability. In this regard, here we demonstrate that *Trf1* genetic deletion in the brain does not affect the cognitive or neuromuscular abilities of mice. Similarly, we did not defect any signs of sickness or morbidity in the xenograft models treated with TRF1 chemical inhibitors compared with the placebo group, supporting a therapeutic window for TRF1 inhibition. A recent report also showed that deletion of the essential shelterin component TRF2 in the brain does not lead to any brain dysfunction (Lobanova et al., 2017).

In summary, we demonstrate here the effectiveness of targeting TRF1 in different mouse glioblastoma subtypes, as well as in patient-derived human xenograft models, in the absence of any detectable deleterious effects for brain function or organismal viability.

STAR★METHODS

Detailed methods are provided in the online version of this paper and include the following:

- KEY RESOURCES TABLE
- CONTACT FOR REAGENT AND RESOURCE SHARING
- EXPERIMENTAL MODEL AND SUBJECT DETAILS
  - Mice
  - Cell Culture and Transfection
  - Neural Stem Cell (NSC) and Glioma Stem Cell (GSC) Isolation and Culture
- METHODS DETAILS
  - Generation of Mouse Models with Brain Tumors
  - Neurosphere Formation Assays
  - Intracranial Cell Transplantation into Syngeneic Mice
  - Xenografts Experiments
  - Telomere Length Analyses on Tissue Sections
  - Cognitive Tests
  - Immunofluorescence Analyses in Cells and Tissue Sections
  - Immunohistochemistry Analyses in Tissue Sections
  - Real-Time qPCR
  - PCR
  - Western-Blots
  - TRF1 Chemical Inhibitors
  - Irradiation and Temozolomide
  - Tissue Micro Array (TMA)
- QUANTIFICATION AND STATISTICAL ANALYSIS

Figure 8. TRF1 Chemical Inhibitors Reduce Stemness and Xenograft Tumor Growth in Patient-Derived Primary GSCs

(A) Representative images (left) and quantification (right) of number of neurospheres formed by h543 and h676 GSCs treated with the indicated compounds. Scale bars, 100 μm.

(B) Xenograft mouse models from patient-derived primary GSCs are generated by subcutaneous injection of GSCs into nude mice. One week after injection, mice are treated either with ETP-47037 or with vehicle as placebo.

(C) Representative image of tumors (left) and longitudinal tumor growth follow-up (right) in ETP-47037- or vehicle-treated xenograft models with h676 GSCs (right).

(D) Representative image of tumors (left) and longitudinal tumor growth follow-up (right) in ETP-47037- or vehicle-treated mice injected with h543 GSCs and representative image of tumors.

(E) Representative image of tumors (left) and tumor weight (right) in ETP-47037- or vehicle-treated mice injected with h676 GSCs at postmortem.

(F) TRF1 nuclear fluorescence in ETP-47037- or vehicle-treated tumors. Scale bars, 5 μm.

(G) Representative images (left) and percentage (right) of Ki67-positive cells per field in ETP-47037- or vehicle-treated tumors. Scale bars, 50 μm.

(H) Representative images (left) and percentage (right) of γH2AX-positive cells per field in in ETP-47037- or vehicle-treated tumors. Scale bars, 50 μm.

Data are represented as mean ± SD. n represents the number of biological replicates in (A) and the number of tumors in (C–H). Statistical analysis: unpaired t test. *$p < 0.05$, **$p < 0.01$, ***$p < 0.001$. See also Figure S8 and Table S1.

SUPPLEMENTAL INFORMATION

Supplemental Information includes eight figure and two tables and can be found with this article online at https://doi.org/10.1016/j.ccell.2017.10.006.

AUTHOR CONTRIBUTIONS

Investigation, L.B.; Writing – Original Draft, M.A.B. and L.B.; Writing – Review & Editing, M.A.B. and L.B.; Resources, A.J.S., M.S., M.M., S.M., C.B.A., J.P., and D.M.; Supervision, M.A.B.

ACKNOWLEDGMENTS

We thank R. Serrano for mice handling, J.M. Flores for histopathology, M. Valiente for the human astrocyte (HA) cell line, and the Comparative Pathology and Biobank Units at CNIO. MAB laboratory is funded by SAF2013-45111-R from MINECO, *Fundación Botín*, and Banco Santander, Worldwide Cancer Research 16-1177. L.B. is a fellow of the La Caixa-Severo Ochoa International PhD Program.

Received: April 19, 2017
Revised: July 28, 2017
Accepted: October 7, 2017
Published: November 13, 2017

REFERENCES

Alt, F.W., Chang, S., Weiler, S.R., Ganesan, S., Chaudhuri, J., Zhu, C., Artandi, S.E., Rudolph, K.L., Gottlieb, G.J., Chin, L., et al. (2000). Telomere dysfunction impairs DNA repair and enhances sensitivity to ionizing radiation. Nat. Genet. *26*, 85–88.

Badie, B., Goh, C.S., Klaver, J., Herweijer, H., and Boothman, D.A. (1999). Combined radiation and p53 gene therapy of malignant glioma cells. Cancer Gene Ther. *6*, 155–162.

Bainbridge, M.N., Armstrong, G.N., Gramatges, M.M., Bertuch, A.A., Jhangiani, S.N., Doddapaneni, H., Lewis, L., Tombrello, J., Tsavachidis, S., Liu, Y., et al. (2015). Germline mutations in shelterin complex genes are associated with familial glioma. J. Natl. Cancer Inst. *107*, 384.

Bao, S., Wu, Q., McLendon, R.E., Hao, Y., Shi, Q., Hjelmeland, A.B., Dewhirst, M.W., Bigner, D.D., and Rich, J.N. (2006). Glioma stem cells promote radioresistance by preferential activation of the DNA damage response. Nature *444*, 756–760.

Beier, F., Foronda, M., Martinez, P., and Blasco, M.A. (2012). Conditional TRF1 knockout in the hematopoietic compartment leads to bone marrow failure and recapitulates clinical features of dyskeratosis congenita. Blood *120*, 2990–3000.

Bernardes de Jesus, B., Vera, E., Schneeberger, K., Tejera, A.M., Ayuso, E., Bosch, F., and Blasco, M.A. (2012). Telomerase gene therapy in adult and old mice delays aging and increases longevity without increasing cancer. EMBO Mol. Med. *4*, 691–704.

Bhat, K.P.L., Balasubramaniyan, V., Vaillant, B., Ezhilarasan, R., Hummelink, K., Hollingsworth, F., Wani, K., Heathcock, L., James, J.D., Goodman, L.D., et al. (2013). Mesenchymal differentiation mediated by NF-κB promotes radiation resistance in glioblastoma. Cancer Cell *24*, 331–346.

Boldrini, L., Pistolesi, S., Gisfredi, S., Ursino, S., Ali, G., Pieracci, N., Basolo, F., Parenti, G., and Fontanini, G. (2006). Telomerase activity and hTERT mRNA expression in glial tumors. Int. J. Oncol. *28*, 1555–1560.

Boué, S., Paramonov, I., Barrero, M.J., and Izpisúa Belmonte, J.C. (2010). Analysis of human and mouse reprogramming of somatic cells to induced pluripotent stem cells. what is in the plate? PLoS One *5*, 1–14.

Bowman, R.L., Wang, Q., Carro, A., Verhaak, R.G., and Squatrito, M. (2017). GlioVis data portal for visualization and analysis of brain tumor expression datasets. Neuro Oncol. *19*, 139–141.

Bryan, T.M., Englezou, A., Dalla-Pozza, L., Dunham, M.A., and Reddel, R.R. (1997). Evidence for an alternative mechanism for maintaining telomere length in human tumors and tumor-derived cell lines. Nat. Med. *3*, 1271–1274.

Calvete, O., Martinez, P., Garcia-Pavia, P., Benitez-Buelga, C., Paumard-Hernández, B., Fernandez, V., Dominguez, F., Salas, C., Romero-Laorden, N., Garcia-Donas, J., et al. (2015). A mutation in the POT1 gene is responsible for cardiac angiosarcoma in TP53-negative Li-Fraumeni-like families. Nat. Commun. *6*, 8383.

Carro, A., Perez-Martinez, M., Soriano, J., Pisano, D.G., and Megias, D. (2015). iMSRC: converting a standard automated microscope into an intelligent screening platform. Sci. Rep. *5*, 10502.

Chen, J., McKay, R.M., and Parada, L.F. (2012). Malignant glioma: lessons from genomics, mouse models, and stem cells. Cell *149*, 36–47.

Chin, L., Artandi, S.E., Shen, Q., Tam, A., Lee, S.L., Gottlieb, G.J., Greider, C.W., and DePinho, R.A. (1999). p53 deficiency rescues the adverse effects of telomere loss and cooperates with telomere dysfunction to accelerate carcinogenesis. Cell *97*, 527–538.

De Lange, T. (2005). Shelterin: the protein complex that shapes and safeguards human telomeres. Genes Dev. *19*, 2100–2110.

El Fassi, D. (2015). Telomerase inhibitor imetelstat in essential thrombocythemia and myelofibrosis. N. Engl. J. Med. *373*, 2579–2581.

Faiz, M., Sachewsky, N., Gascón, S., Bang, K.W., Morshead, C.M., and Nagy, A. (2015). Adult neural stem cells from the subventricular zone give rise to reactive astrocytes in the cortex after stroke. Cell Stem Cell *17*, 624–634.

Fang, X., Zhou, W., Wu, Q., Huang, Z., Shi, Y., Yang, K., Chen, C., Xie, Q., Mack, S.C., Wang, X., et al. (2017). Deubiquitinase USP13 maintains glioblastoma stem cells by antagonizing FBXL14-mediated Myc ubiquitination. J. Exp. Med. *214*, 245–267.

García-Beccaria, M., Martínez, P., Méndez-Pertuz, M., Martínez, S., Blanco-Aparicio, C., Cañamero, M., Mulero, F., Ambrogio, C., Flores, J.M., Megias, D., et al. (2015). Therapeutic inhibition of TRF1 impairs the growth of p53-deficient K-RasG12V-induced lung cancer by induction of telomeric DNA damage. EMBO Mol. Med. *7*, 930–949.

Gonzalez-Suarez, E., Samper, E., Flores, J.M., and Blasco, M.A. (2000). Telomerase-deficient mice with short telomeres are resistant to skin tumorigenesis. Nat. Genet. *26*, 114–117.

Goytisolo, F.A., Samper, E., Martín-Caballero, J., Finnon, P., Herrera, E., Flores, J.M., Bouffler, S.D., and Blasco, M.A. (2000). Short telomeres result in organismal hypersensitivity to ionizing radiation in mammals. J. Exp. Med. *192*, 1625–1636.

Greider, C.W., and Blackburn, E.H. (1985). Identification of a specific telomere terminal transferase activity in tetrahymena extracts. Cell *43*, 405–413.

Hambardzumyan, D., Amankulor, N.M., Helmy, K.Y., Becher, O.J., and Holland, E.C. (2009). Modeling adult gliomas using RCAS/t-va technology. Transl. Oncol. *2*, 89–95.

Hanahan, D., and Weinberg, R.A. (2011). Hallmarks of cancer: the next generation. Cell *144*, 646–674.

Harley, C.B., Futcher, A.B., and Greider, C.W. (1990). Telomeres shorten during ageing of human fibroblasts. Nature *345*, 458–460.

Hasegawa, D., Okabe, S., Okamoto, K., Nakano, I., Shin-ya, K., and Seimiya, H. (2016). G-quadruplex ligand-induced DNA damage response coupled with telomere dysfunction and replication stress in glioma stem cells. Biochem. Biophys. Res. Commun. *471*, 75–81.

Heaphy, C.M., de Wilde, R.F., Jiao, Y., Klein, A.P., Edil, B.H., Shi, C., Bettegowda, C., Rodriguez, F.J., Eberhart, C.G., Hebbar, S., et al. (2011). Altered telomeres in tumors with ATRX and DAXX mutations. Science *333*, 425.

Holland, E.C., Hively, W.P., DePinho, R.A., and Varmus, H.E. (1998). A constitutively active epidermal growth factor receptor cooperates with disruption of G1 cell-cycle arrest pathways to induce glioma-like lesions in mice. Genes Dev. *12*, 3675–3685.

Hu, H., Zhang, Y., Zou, M., Yang, S., and Liang, X.Q. (2010). Expression of TRF1, TRF2, TIN2, TERT, KU70, and BRCA1 proteins is associated with telomere shortening and may contribute to multistage carcinogenesis of gastric cancer. J. Cancer Res. Clin. Oncol. *136*, 1407–1414.

Jiang, Y., Boije, M., Westermark, B., and Uhrbom, L. (2011). PDGF-B can sustain self-renewal and tumorigenicity of experimental glioma-derived cancer-initiating cells by preventing oligodendrocyte differentiation. Neoplasia *13*, 492–503.

Kanzawa, T., Germano, I.M., Kondo, Y., Ito, H., Kyo, S., and Kondo, S. (2003). Inhibition of telomerase activity in malignant glioma cells correlates with their sensitivity to temozolomide. Br. J. Cancer *89*, 922–929.

Kim, N., Piatyszek, M.A., Prowse, K.R., Harley, C.B., West, M.D., Ho, P.L., Coviello, G.M., Wright, W.E., Weinrich, S.L., and Shay, J.W. (1994). Specific association of human telomerase activity with immortal cells and cancer. Science *266*, 2011–2015.

Lathia, J.D., Mack, S.C., Mulkearns-Hubert, E.E., Valentim, C.L., and Rich, J.N. (2015). Cancer stem cells in glioblastoma. Genes Dev. *29*, 1203–1217.

Liu, D., O'Connor, M.S., Qin, J., and Songyang, Z. (2004). Telosome, a mammalian telomere-associated complex formed by multiple telomeric proteins. J. Biol. Chem. *279*, 51338–51342.

Lobanova, A., She, R., Pieraut, S., Clapp, C., Maximov, A., and Denchi, E.L. (2017). Different requirements of functional telomeres in neural stem cells and terminally differentiated neurons. Genes Dev. *31*, 639–647.

Louis, D.N., Ohgaki, H., Wiestler, O.D., Cavenee, W.K., Burger, P.C., Jouvet, A., Scheithauer, B.W., and Kleihues, P. (2007). The 2007 WHO Classification of Tumours of the Central Nervous System. Acta Neuropathol. *114*, 97, 114, 547.

Marian, C.O., Cho, S.K., McEllin, B.M., Maher, E.A., Hatanpaa, K.J., Madden, C.J., Mickey, B.E., Wright, W.E., Shay, J.W., and Bachoo, R.M. (2010). The telomerase antagonist, imetelstat, efficiently targets glioblastoma tumor-initiating cells leading to decreased proliferation and tumor growth. Clin. Cancer Res. *16*, 154–163.

Marion, R.M., Strati, K., Li, H., Tejera, A., Schoeftner, S., Ortega, S., Serrano, M., and Blasco, M.A. (2009). Telomeres acquire embryonic stem cell characteristics in induced pluripotent stem cells. Cell Stem Cell *4*, 141–154.

Martínez, P., and Blasco, M.A. (2011). Telomeric and extra-telomeric roles for telomerase and the telomere-binding proteins. Nat. Rev. Cancer *11*, 161–176.

Martínez, P., Thanasoula, M., Muñoz, P., Liao, C., Tejera, A., McNees, C., Flores, J.M., Fernández-Capetillo, O., Tarsounas, M., and Blasco, M.A. (2009). Increased telomere fragility and fusions resulting from TRF1 deficiency lead to degenerative pathologies and increased cancer in mice. Genes Dev. *23*, 2060–2075.

Middleton, G., Silcocks, P., Cox, T., Valle, J., Wadsley, J., Propper, D., Coxon, F., Ross, P., Madhusudan, S., Roques, T., et al. (2014). Gemcitabine and capecitabine with or without telomerase peptide vaccine GV1001 in patients with locally advanced or metastatic pancreatic cancer (TeloVac): an open-label, randomised, phase 3 trial. Lancet Oncol. *15*, 829–840.

Mignone, J.L., Kukekov, V., Chiang, A.S., Steindler, D., and Enikolopov, G. (2004). Neural stem and progenitor cells in nestin-GFP transgenic mice. J. Comp. Neurol. *469*, 311–324.

Nonoguchi, N., Ohta, T., Oh, J.E., Kim, Y.H., Kleihues, P., and Ohgaki, H. (2013). TERT promoter mutations in primary and secondary glioblastomas. Acta Neuropathol. *126*, 931–937.

Ozawa, T., Riester, M., Cheng, Y.K., Huse, J.T., Squatrito, M., Helmy, K., Charles, N., Michor, F., and Holland, E.C. (2014). Most human non-GCIMP glioblastoma subtypes evolve from a common proneural-like precursor glioma. Cancer Cell *26*, 288–300.

Pal, D., Sharma, U., Singh, S.K., Kakkar, N., and Prasad, R. (2015). Overexpression of telomere binding factors (TRF1 & TRF2) in renal cell carcinoma and their inhibition by using SiRNA induce apoptosis, reduce cell proliferation and migration in vitro. PLoS One *10*, e0115651.

Parkhurst, M.R., Riley, J.P., Igarashi, T., Li, Y., Robbins, P.F., and Rosenberg, S.A. (2004). Immunization of patients with the hTERT:540-548 peptide induces peptide-reactive T lymphocytes that do not recognize tumors endogenously expressing telomerase. Clin. Cancer Res. *10*, 4688–4698.

Ramsay, A.J., Quesada, V., Foronda, M., Conde, L., Martínez-Trillos, A., Villamor, N., Rodríguez, D., Kwarciak, A., Garabaya, C., Gallardo, M., et al. (2013). POT1 mutations cause telomere dysfunction in chronic lymphocytic leukemia. Nat. Genet. *45*, 526–530.

Robles-Espinoza, C.D., Harland, M., Ramsay, A.J., Aoude, L.G., Quesada, V., Ding, Z., Pooley, K.A., Pritchard, A.L., Tiffen, J.C., Petljak, M., et al. (2014). POT1 loss-of-function variants predispose to familial melanoma. Nat. Genet. *46*, 478–481.

Rohle, D., Popovici-Muller, J., Palaskas, N., Turcan, S., Grommes, C., Campos, C., Tsoi, J., Clark, O., Oldrini, B., Komisopoulou, E., et al. (2013). An inhibitor of mutant IDH1 delays growth and promotes differentiation of glioma cells. Science *340*, 626–630.

Ruzankina, Y., Pinzon-Guzman, C., Asare, A., Ong, T., Pontano, L., Cotsarelis, G., Zediak, V.P., Velez, M., Bhandoola, A., and Brown, E.J. (2007). Deletion of the developmentally essential gene ATR in adult mice leads to age-related phenotypes and stem cell loss. Cell Stem Cell *1*, 113–126.

Schneider, R.P., Garrobo, I., Foronda, M., Palacios, J.A., Marión, R.M., Flores, I., Ortega, S., and Blasco, M.A. (2013). TRF1 is a stem cell marker and is essential for the generation of induced pluripotent stem cells. Nat. Commun. *4*, 1946.

Serrano, M., Lee, H., Chin, L., Cordon-Cardo, C., Beach, D., and DePinho, R.A. (1996). Role of the INK4a locus in tumor suppression and cell mortality. Cell *85*, 27–37.

Sfeir, A., Kosiyatrakul, S.T., Hockemeyer, D., MacRae, S.L., Karlseder, J., Schildkraut, C.L., and de Lange, T. (2009). Mammalian telomeres resemble fragile sites and require TRF1 for efficient replication. Cell *138*, 90–103.

Shay, J.W., and Bacchetti, S. (1997). A survey of telomerase activity in human cancer. Eur. J. Cancer *33*, 787–791.

Singh, S.K., Hawkins, C., Clarke, I.D., Squire, J.A., Bayani, J., Hide, T., Henkelman, R.M., Cusimano, M.D., and Dirks, P.B. (2004). Identification of human brain tumour initiating cells. Nature *432*, 396–401.

Soeda, A., Hara, A., Kunisada, T., Yoshimura, S., Iwama, T., and Park, D.M. (2015). The evidence of glioblastoma heterogeneity. Sci. Rep. *5*, 7979.

Tejera, A.M., Stagno d'Alcontres, M., Thanasoula, M., Marion, R.M., Martinez, P., Liao, C., Flores, J.M., Tarsounas, M., and Blasco, M.A. (2010). TPP1 is required for TERT recruitment, telomere elongation during nuclear reprogramming, and normal skin development in mice. Dev. Cell *18*, 775–789.

Tomás-Loba, A., Flores, I., Fernández-Marcos, P.J., Cayuela, M.L., Maraver, A., Tejera, A., Borrás, C., Matheu, A., Klatt, P., Flores, J.M., et al. (2008). Telomerase reverse transcriptase delays aging in cancer-resistant mice. Cell *135*, 609–622.

Wen, P.Y., and Kesari, S. (2008). Malignant gliomas in adults. N. Engl. J. Med. *359*, 492–507.

Yang, M., and Crawley, J.N. (2009). Simple behavioral assessment of mouse olfaction. Curr. Protoc. Neurosci. *Chapter 8*. Unit 8.24.

STAR★METHODS

KEY RESOURCES TABLE

REAGENT or RESOURCE	SOURCE	IDENTIFIER
Antibodies		
Mouse monoclonal anti-Nestin	BD Pharmigen	Cat# 556309; RRID: AB_396354
Rabbit polyclonal anti-RAP1 (BL735)	Bethyl	Cat#A300-306A; RRID: AB_162721
Rat polyclonal anti-TRF1	Homemade	N/A
Mouse monoclonal anti-TRF1 (BED5)	Cell Signaling	Cat#3529; RRID: AB_2201452
Mouse monoclonal anti-TRF1 (TRF-78)	ABCAM	Cat# ab10579; RRID: AB_2201461
Mouse monoclonal anti-γH2AX (Ser139) (JBW301)	Millipore	Cat#05-636; RRID: AB_309864
Rabbit polyclonal anti-53BP1	Novus Biologicals	Cat#NB100-304; RRID: AB_10003037
Mouse monoclonal anti-HA tag (6E2)	Cell Signaling	Cat#2367; RRID: AB_2314619
Mouse monoclonal anti-MYC tag (9E10)	Santa Cruz	Cat#SC-40
Rabbit monoclonal anti-Ki67	Master diagnostica	Cat#0003110QD
Rabbit polyclonal anti-p-RPA32 (S4/S8)	Bethyl	Cat# A300-245A; RRID: AB_210547
Rat monoclonal anti-p53 (POE316 A/E9)	Homemade	N/A
Rat monoclonal anti-p21 (291H/B5)	Homemade	N/A
Rabbit polyclonal anti-AC3 (Asp175)	Cell Signaling	Cat# 9661; RRID: AB_2341188
Mouse monoclonal anti-NF1 (E-8)	Santa Cruz	Cat# sc-398267
Rabbit polyclonal anti-TRF2	Novus Biologicals	Cat# NB110-57130; RRID: AB_844199
Biological Samples		
Tissue microarray Astrocytoma and Glioblastoma	CNIO Biobank	TA-371
Tissue microarray TA-Normal Brain Tissue	CNIO.Biobank	TA-438
Chemicals, Peptides, and Recombinant Proteins		
ETP-47228	CNIO	(García-Beccaria et al., 2015)
ETP-47037	CNIO	(García-Beccaria et al., 2015)
ETP-50946	CNIO	N/A
Temozolomide		
4-HydroTamoxifen	Sigma	Cat#H6278-50MG
Epidermal Growth Factor (EGF)	Life Technologies	Cat#PHG0313
Basic Fibroblast Growth Factor (bFGF)	Vitro	Cat# 233-FB-025/CF
Laminin	Life Technologies	Cat# L2020-1MG
Heparin	Stemcell	Cat# 07980
Critical Commercial Assays		
Nuclear Cytosolic Fractionation Kit	Biovision	Cat# K266-100
NeuroCult™ Proliferation Kit (Human)	Stemcell	Cat# 05751
NeuroCult™ Proliferation Kit (Mouse)	Stemcell	Cat#05702
Experimental Models: Cell Lines		
Human astrocytes (HA)	ScienceCell	Cat#1800
U251	Kindly provided by Eric Holland's lab	N/A
U87	ATCC	Cat# HTB-14
T98G	Kindly provided by Eric Holland's lab	N/A
DF1 chicken fibroblasts	ATCC	Cat# CRL-12203
h676	(Ozawa et al., 2014; Rohle et al., 2013)	N/A
h543	Ozawa et al., 2014; Rohle et al., 2013)	N/A
Experimental Models: Organisms/Strains		
Mouse: *Nestin-Tva*	(Holland et al., 1998)	N/A
Mouse: *Ink4Arf*$^{-/-}$	(Serrano et al., 1996	N/A

(*Continued on next page*)

Continued		
REAGENT or RESOURCE	SOURCE	IDENTIFIER
Mouse: *TRF1*$^{lox/lox}$	(Martínez et al., 2009)	N/A
Mouse: *hUBC-CreERT2*	Ruzankina et al., 2007)	N/A
Hsd: athymic Nude-Foxn1nu	Harlan	N/A
Oligonucleotides		
See Table S2		
Software and Algorithms		
Definiens	N/A	N/A
iMSRC	N/A	N/A
ImageJ	N/A	N/A
NIS Elements Basic Research	N/A	N/A

CONTACT FOR REAGENT AND RESOURCE SHARING

Further information and requests for resources and reagents should be directed to and will be fulfilled by the Lead Contact, Maria Blasco (mblasco@cnio.es).

EXPERIMENTAL MODEL AND SUBJECT DETAILS

Mice

Nestin-Tva (Holland et al., 1998; Hambardzumyan et al., 2009), *Cdkn2a*$^{-/-}$ (Serrano et al., 1996) and *Trf1*$^{lox/lox}$ (Martínez et al., 2009) mice where crossed to obtain the *Trf1*$^{lox/lox}$ Nestin-Tva *Cdkn2a*$^{-/-}$ or *Trf1*$^{+/+}$ Nestin-Tva *Cdkn2a*$^{-/-}$ mouse models used for tumor initiation experiments. This mouse models were crossed with a mouse strain carrying ubiquitously expressed, tamoxifen-activated recombinase, *hUBC-CreERT2* (Ruzankina et al., 2007) to generate *Trf1*$^{lox/lox}$*;hUBC-CreERT2*;Nestin-Tva;*Cdkn2a*$^{-/-}$ and *Trf1*$^{+/+}$*;hUBC-CreERT2*;Nestin-Tva;*Cdkn2a*$^{-/-}$ mice. These mice received intraperitoneal injections of tamoxifen (2 mg/injection, 4-6 injections) for short-term experiments or they were fed *ad libitum* with tamoxifen containing diet for long-term experiments. All mice were maintained at the Spanish National Cancer Centre under specific pathogen-free conditions in accordance with the recommendations of the Federation of European Laboratory Animal Science Associations (FELASA). All animal experiments were approved by the Ethical Committee (CEIyBA) from the Spanish National Cancer Centre and performed in accordance with the guidelines stated in the International Guiding Principles for Biomedical Research Involving Animals, developed by the Council for International Organizations of Medical Sciences (CIOMS).

Cell Culture and Transfection

Human astrocytes (HA), U251 cells, U87 cells, T98G cells, 293T cells and DF1 cells (ATCC) were grown at 37°C in 10% FBS (GIBCO) containing DMEM (GIBCO). DF1 cells were transfected with the RCAS-Cre, RCAS-PDGFB-HA, RCAS-PDGFA-MYC, RCAS-GFP-shNf1 or RCAS-RFP-shp53 viral plasmids using Fugene 6 Transfection reagent (Roche), accordingly to manufacture protocol.

pGIPZ lentiviral TRF1 shRNAs and pGIPZ-scrambled shRNA were introduced in the U251 glioma cell line using standard lentiviral infection procedures.

Neural Stem Cell (NSC) and Glioma Stem Cell (GSC) Isolation and Culture

NSCs were obtained by neonatal brain digestion with papain (Worthington). GSCs were extracted from mice tumors using the same procedure. Both mice NSC and GSC were cultured in neurosphere medium from NeuroCult (Stem Cell Technologies Inc, Vancouver, Canada) supplemented with 10 ng/ml EGF (Gibco), 20 ng/ml basic-FGF (RD Systems) and 1mg/ml Heparin (Stem Cell Technologies). Patient-derived h543 and h676 GSCs have been previously used (Ozawa et al., 2014; Rohle et al., 2013). These cells were also cultured in neurosphere medium from NeuroCult (Stem Cell Technologies Inc, Vancouver, Canada) supplemented with 10 ng/ml EGF (Life Technologies, S.A.), 20 ng/ml basic-FGF (VITRO, S.A.) and 1mg/ml Heparin (Stem Cell Technologies).

Cells were grown in suspension or in adhesion in laminin (Life Technologies) coated plates.

METHODS DETAILS

Generation of Mouse Models with Brain Tumors

The RCAS/tv-a system used in this work has been described previously (Holland et al., 1998; Hambardzumyan et al., 2009). Adult mice (4.5-6 weeks old) were injected in the SVZ with 1 ul of DF-1 chicken fibroblasts producing RCAS-Cre, RCAS-PDGFB-HA, RCAS-PDGFA-MYC, RCAS-GFP-shNf1 or RCAS-RFP-shp53 as described at a concentration of 200.000 cells/ul, with the exception

of RCAS-Cre producing cells that where injected at a concentration of 600.000 cell/ul. All mice were monitored and killed whenever they presented symptoms of brain tumor development. For all studies we used both male and female mice.

Neurosphere Formation Assays

Spheres were dissociated into single cells and seeded at a density of 50, 100, 200 and 400 cells/well in a 96 well plate. Neurosphere number was assed after 7 days. Pictures were taken using Nikon Eclipse Ti-U microscope and neurosphere diameter was measured using NIS Elements BR software.

Intracranial Cell Transplantation into Syngeneic Mice

Spheres were dissociated using a 200 ul pippet and were resuspended in a concentration of 100.000 cells/μl. From these aliquots, 1 μl was injected into the brain of adult syngeneic mice. All mice were monitored and killed whenever they presented symptoms of brain tumor development.

Xenografts Experiments

h676 and h543 patient-derived GSCs were dissociated using a 200 μl pipet and resuspendend in NeuroCult medium and matrigel in a 1:1 ratio in a concentration of 1000 cells/μl. Nude mice (Hsd: athymic Nude-Foxn1nu from Harlan France) were injected subcutaneously with 100 μl of the cell preparation. ETP-47037 (or vehicle) was orally administrated at a concentration of 75 mg/kg 5 days per weeks for a total of 2 weeks, starting one week after cell injection. The vehicle consisted in 10% *N*-methyl-2-pyrrolidone (NMP, Sigma Aldrich) and 90% poly ethylene glycol (PEG, Sigma Aldrich). Mice were weighted and tumors were measured every 2-4 days. Tumor area was determined by the following equation: $A = \pi * (a/2) * (b/2)$, were *a* and *b* are tumor length and width respectively.

Telomere Length Analyses on Tissue Sections

For quantitative telomere fluorescence *in situ* hybridization (Q-FISH) paraffin-embedded sections were deparaffinized and fixed with 4% formaldehyde, followed by digestion with pepsine/HCl and a second fixation with 4% formaldehyde. Slides were dehydrated with increasing concentrations of EtOH (70%, 90%, 100%) and incubated with the telomeric probe for 3.5 min at 85°C followed by 2h RT incubation in a wet chamber. In the final steps, the slides were extensively washed with 50% formamide and 0.08% TBS-Tween. Analysis was performed by Definiens software.

Cognitive Tests

To evaluate memory skills, mice were tested by the object recognition test (Bernardes de Jesus et al., 2012). A total of two 3 different objects were used for the test, two identical objects (A) and a third different object (B). In day 1, mice were placed in a box with the two identical objects for 10 minutes. In day 2, one of the objects was replaced by object B and the mice were again placed for ten minutes and recorded with a camera. Analysis was made by calculating time spent with object B divided with time spent with (A+B).

To check the ability to smell, mice were tested by the buried food test (Yang and Crawley, 2009). Mice were fasted for 24 hr and they were placed in a cage with a buried pellet food. Analysis was made by calculating the percentage of success and the time spent to find the food pellet.

To measure coordination and balance, mice were tested in a Rotarod apparatus (model LE 8200) and with the tightrope test. In the rotarod test we measured the time mice could stay on the rod. In the tightrope test, we evaluate the ability of the mice to stay in the rope without falling, and we considered a ‘‘success’’ if mice were able to stay more than one minute.

Immunofluorescence Analyses in Cells and Tissue Sections

For immunofluorescence analyses, cells were plated in a proper density in cell culture μCLEAR plates (Greiner) and fixed in 4% formaldehyde in PBS. Cells were permeabilized with 0.25% Triton in PBS and blocked with 5% BSA in PBS.

Tissue sections were fixed in 10% buffered formalin (Sigma) and embedded in paraffin. After despparafination and citrate antigen retrieval, section were permeabilized with 0.5% Triton in PBS and blocked with 1%BSA and 10% Australian FBS (GENYCELL) in PBS.

The antibodies were applied overnight in antibody diluents with background reducing agents (Invitrogen).

Primary Antibodies

Anti-Nestin (BD Pharmigen), anti-Rap1 (BL735, Bethyl), rat polyclonal anti-TRF1 (homemade), anti-TRF1 (BED5, Cell Signaling), anti-γH2AX Ser139 (05-636, Millipore), anti-53BP1 (Novus Biologicals), anti-HA tag (Cell Signaling Technology), anti-MYC-tag (9E10, Santa Cruz), anti-Ki67 (Master diagnostica), anti-p-RPA32 (S4/S8) (Bethly).

Immunofluorescence images were obtained using a confocal ultraspectral microscope (Leica TCS-SP5) or the Opera High Content Screening (HCS) system (Perkin Elmer). Quantifications were performed with Definiens software.

Immunohistochemistry Analyses in Tissue Sections

Antibodies used for immunohistochemistry included those raised against: γH2AX Ser 139 (Millipore), Ki67 (Master diagnostica), HA tag (Cell Signaling Technology), p53 (POE316A/E9, homemade), p21 (291H/B5, homemade), AC3 (Cell Signaling Technology), NF-1 (Santa Cruz Biotechnology).

Pictures were taken using Olympus AX70 microscope. The percentage of positive cells was identified by eye and the areas were calculated by CellSens Entry software.

Real-Time qPCR

Total RNA from cells was extracted with the RNeasy kit (QIAGEN) and reverse transcribed was using the iSCRIPT cDNA synthesis kit (BIO-RAD) according to manufacturés protocols.

Quantitative real-time PCR was performed with the QuantStudio 6 Flex (Applied Biosystems, Life Technologies) using Go-Taq qPCR master mix (Promega) according to the manufacturers protocol. All values were obtained in triplicates.

Primers for mouse and human samples are listed in Table S2.

PCR

DNA of cells and tissue samples was extracted using Phenol:Chloroform:Isoamyl:Alcohol (Sigma). We determined Cre-mediated recombination by PCR using the following primers:

F: 5′-ATAGTGATCAAAATGTGGTCCTGGG-3′

R: 5′-GCTTGCCAAATTGGGTTGG-3′

Western-Blots

Nuclear protein extracts were obtained using Nuclear Cytosolic Fractionation Kit (Biovision) and protein concentration was determined using the Bio-Rad DC Protein Assay (Bio-Rad). Up to fifteen micrograms of protein per extract were separated in SDS–polyacrylamide gels by electrophoresis. After protein transfer onto nitrocellulose membrane (Whatman), the membranes were incubated with the indicated antibodies. Antibody binding was detected after incubation with a secondary antibody coupled to horseradish peroxidase using chemiluminescence with ECL detection KIT (GE Healthcare)

Primary Antibodies

Anti-TRF1 (BED5, Cell Signaling), anti-TRF1 (TRF-78, Abcam), anti-TRF2 (Novus Biologicals), anti-RAP1 (Bethyl) anti-SMC-1 (Bethyl), anti-βACTIN (Sigma).

Quantifications: Protein-band intensities were measured with ImageJ software and normalized against the loading control.

TRF1 Chemical Inhibitors

ETP-47228 ETP-47037 chemical compounds have been described previously (García-Beccaria et al., 2015). ETP-50946 is the result of the enantiomeric separation of a racemic compound included into a Kinase Inhibitor Library sourced from BioFocus (Galapagos, Belgium) (Figure 7A).

For *in vitro* studies, ETP-47228 ETP-47037 and ETP-50946 were dissolved in DMSO at a final concentration of 10 or 5 mM. Cells were treated at a concentration of 10 μM for 24 hr or 48 hr.

For oral administration, ETP-47037 was dissolved in 10% *N*-methyl-2-pyrrolidone (NMP, Sigma Aldrich) and 90% poly ethylene glycol (PEG, Sigma Aldrich) at a concentration of 75 mg/kg.

Irradiation and Temozolomide

Cells were irradiated with 6Gy using the irradiation apparatus MDS Nordion Gamma Cells 1000. Cells were treated with temozolomide at a concentration of 500 μM or 1000 μM for three days.

Tissue Micro Array (TMA)

The TMAs TA- 371 and TA-438 where obtained from the CNIO Biobank. The use of this samples has been approved by the Ethical Committee (CEI) of the Spanish National Cancer Centre. TMA acquisition was performed with a TCS SP5 confocal microscope (Leica Microsystems) equipped with Leica HCS-A and the custom-made iMSRC software (Carro et al., 2015). Final images were acquired with a 40x 1.2 N.A. oil immersion Objective.

QUANTIFICATION AND STATISTICAL ANALYSIS

Survival data were analyzed by Kaplan Meier survival curves, and comparisons were performed by Log Rank test. Statistical analysis was performed using GraphPad Prism 5.03. Comparison of the percentage of mice with GBM in Figure 2 was performed by Chi-Square test.

Immunofluorescence quantifications were performed with Definiens software and immunohistochemistry quantifications were performed by direct cell counting. Western Blot protein-band intensities were measured with ImageJ software and normalized against the loading control. Unpaired Student's t test (two-tailed) was used to determine statistical significance. P values of less than 0.05 were considered significant. Statistical analysis was performed using Microsoft® Excel 2011.